CHALMERS
UNIVERSITY OF TECHNOLOGY

Electrical percolation in graphene-polymer composites

2D Materials

OPEN ACCESS

TOPICAL REVIEW

Electrical percolation in graphene–polymer composites

A J Marsden[1], D G Papageorgiou[1], C Vallés[1], A Liscio[2,3], V Palermo[2,4], M A Bissett[1], R J Young[1] and I A Kinloch[1]

[1] National Graphene Institute and School of Materials, Oxford Road, The University of Manchester, Manchester, M13 9PL, United Kingdom
[2] Consiglio Nazionale delle Ricerche, Istituto per la Sintesi Organi e la Fotoreattività, (CNR-ISOF), via Gobetti 101, 40129 Bologna, Italy
[3] Consiglio Nazionale delle Ricerche, Istituto per la Microelettronica e Microsistemi, (CNR-IMM), via del Fosso del Cavaliere 100, 00133 Roma, Italy
[4] Department of Industrial and Materials Science, Chalmers University of technology, 412 96 Gothenburg, Sweden

E-mail: alex.marsden@manchester.ac.uk **and** ian.kinloch@manchester.ac.uk

RECEIVED
20 February 2018

REVISED
5 April 2018

ACCEPTED FOR PUBLICATION
26 April 2018

PUBLISHED
1 June 2018

Keywords: graphene, polymer, composites, conductivity, graphene oxide

Abstract

Electrically conductive composites comprising polymers and graphene are extremely versatile and have a wide range of potential applications. The conductivity of these composites depends on the choice of polymer matrix, the type of graphene filler, the processing methodology, and any post-production treatments. In this review, we discuss the progress in graphene–polymer composites for electrical applications. Graphene filler types are reviewed, the progress in modelling these composites is outlined, the current optimal composites are presented, and the example of strain sensors is used to demonstrate their application.

1. Introduction

A composite is a material that consists of two or more materials or phases, whose final properties differ from those of the original materials. Polymers are extremely versatile materials that make good matrices (or hosts) in composites due to their extensive range of properties and processability. However, in almost all cases pure polymers are insulating, and this limits their application in some sectors. Adding conductive fillers to the polymer matrix yields composites that are also conductive, and these composites have many applications including conductive adhesives [1], lightning strike protection [2], electromagnetic shielding [3], anti-static components [4], and strain sensors [5].

Traditional carbon-based fillers (such as carbon nanotubes (CNTs) [6] and carbon black (CB) [7]) make excellent candidates for conductive composites because of their high electrical conductivity combined with good mechanical properties. In the case of CNTs, they also posses high aspect ratios, which leads to electrically conductive composites at low CNT loadings [8]. However, there are limitations. While low percolation thresholds have been observed, achieving a high ultimate conductivity requires a greater loading of filler, and this often makes the composite brittle and unsuitable for many applications [9–11]. Therefore, alternative fillers are being sought.

Graphene has attracted significant scientific attention as a potential conductive filler. Graphene is a two-dimensional sheet of carbon atoms, sp^2-bonded into a hexagonal arrangement [12]. It has an exciting combination of properties [13], amongst which is its superb electrical conductivity (6×10^5 S m^{-1} [14]) when in a suitable isolated environment. There is now a family of graphene-related materials (GRMs), which differ from pure graphene in that they may contain multiple stacked layers (such as graphene nanoplatelets), or different chemical structures (such as graphene oxide). As composites have become a focus for industrial applications of graphene, these GRMs have drawn the most attention as fillers in graphene composites. Crucially, the structural differences between GRMs and pristine graphene affect the performance of the resulting composite.

There are also many other factors that impact a composite's electrical performance. There are different processing methods including graphene production methods and post-production routines. A careful understanding of each of these is required to achieve the ultimate performance improvements.

Herein we review the recent progress in the understanding of charge percolation in graphene-based polymer composites and how this science has led to performance improvements in these materials. Firstly, we discuss the intrinsic conductive properties of GRMs produced through different routes, high-

lighting how the production route strongly influences the resulting electrical properties. Next, the theoretical aspects of electrical percolation are presented. We then review recent results on the electrical properties of graphene-based composites, summarising the reported composite conductivities as a function of fabrication method and graphene type (these results are generally post-2010, with results before then covered in previous reviews [15, 16]). Finally, as an example of how these developments can be applied, the effect of strain on conducting composites is explored.

2. Electrical conductivity of different types of graphene

2.1. Pristine graphene

The extremely high conductivity of monolayer graphene is one of its most attractive properties. This conductivity arises from the combination of both the high charge carrier mobility and the high charge carrier concentration present in doped graphene. The conductivity, however, is very sensitive to the material's environment and quality. For example, the interaction of graphene with its substrate has a significant influence, with the highest conductivity (6×10^5 S m^{-1}) being measured on suspended sheets [14]. Furthermore, such measurements were performed on high quality, mechanically exfoliated graphene; a method that is not suitable for industrial scale production. There are now many alternative options for producing graphene, most of which are more scalable than mechanical exfoliation, but each method comes with some deterioration of graphene's properties and a struggle to make pure monolayer flakes. There are also further challenges classifying these production methods, so broad categories of GRMs are outlined below.

2.2. Chemical vapour deposition

Chemical vapour deposition (CVD) can produce large areas of monolayer [17] or multilayer [18] graphene depending on the growth conditions and substrate used. The measured conductivities of CVD graphene are lower than those of mechanically exfoliated graphene due mainly to its polycrystalline nature with the boundaries between grains scattering charges [19] and reducing the conductivity. However, recent developments have established growing single-crystal graphene [20, 21]. For example, growing graphene via CVD on single crystals of copper yielded graphene that displayed conductive behaviour without backscattering, because the formation of defects and grain boundaries was suppressed [22]. However, a key limitation of CVD graphene is that growth on metal substrates is still the most dominant route, and transferring graphene from these substrates brings significant challenges [23].

2.3. Graphene oxide and its reduced derivatives

Graphene oxide (GO) is a highly-functionalised and well-exfoliated form of graphene with large lateral dimensions. It is produced through the chemical oxidation of graphite, using the Hummers' [24], Brodie's [25], or Staudenmaier's [26] methods, or more modern modified versions that are less polluting and safer [27]. GO consists of heavily oxygenated graphene sheets that contain hydroxyl, epoxide, diols, ketones and carboxyls functional groups on its surface, as shown in figure 1(a) [28]. The covalent functionalisation of GO has a detrimental impact on its conductivity with reported values generally in the range of 2×10^{-2} S m^{-1} [29], significantly lower than those of graphene, and this renders GO unsuitable for most conductive applications.

The covalent functionalisation of GO, however, is reversible to a certain extent, and some electrical conductivity can be recovered. Most work has shown that the conductivity of GO increases with the reduction of oxygen [30, 31]. At the initial stages of reduction, the conductivity is dominated by tunnelling and hopping between pristine patches of graphene within the sheet. At more advanced levels of reduction, the patches become more connected and transport proceeds via percolation [30]. Reduction procedures (yielding reduced graphene oxide, rGO) consist of thermal treatments (thermally reduced GO, TRGO), or chemical treatments (chemically reduced, CRGO), or a combination of both. The changes to the structure of GO as it is reduced are summarised in figure 1(a).

Chemical reduction of aqueous GO dispersions often uses reducing agents such as hydrazine, sodium borohydride, hydroquinone, various alcohols, sulfur-containing compounds, or even vitamin C [34, 35]. These yield rGO with less oxygen functionalities, a more restored sp^2 network, and an increased electrical conductivity. For example, a bulk powder of CRGO formed after exposure to hydrazine recovered a conductivity of 200 S m^{-1} [29]. Similar values were also obtained from individual monolayers (50–200 S m^{-1}) [36]. Another chemical treatment has been reported that involved immersion in FeI_2 at 95 °C, which recovered a conductivity of 6×10^4 S m^{-1} [37].

Electrochemical reduction through a voltage-induced approach has also been proposed. This has been used to reduce GO (in single sheets and thin films) by applying a potential (pulses of 6 V) between the tip of a conductive atomic force microscope (c-AFM) and a counter-electrode on the substrate surface [38] or between two interdigitated microelectrodes [39] in ambient condition. The reduction results from an electrochemical process whereby hydrogen ions are generated through the oxidation of water present as a thin adsorbed layer at the GO surface. This approach recovered a conductivity of ~1 S m^{-1}, making it possible to engineer rGO micro-devices and micro-circuits in a few minutes.

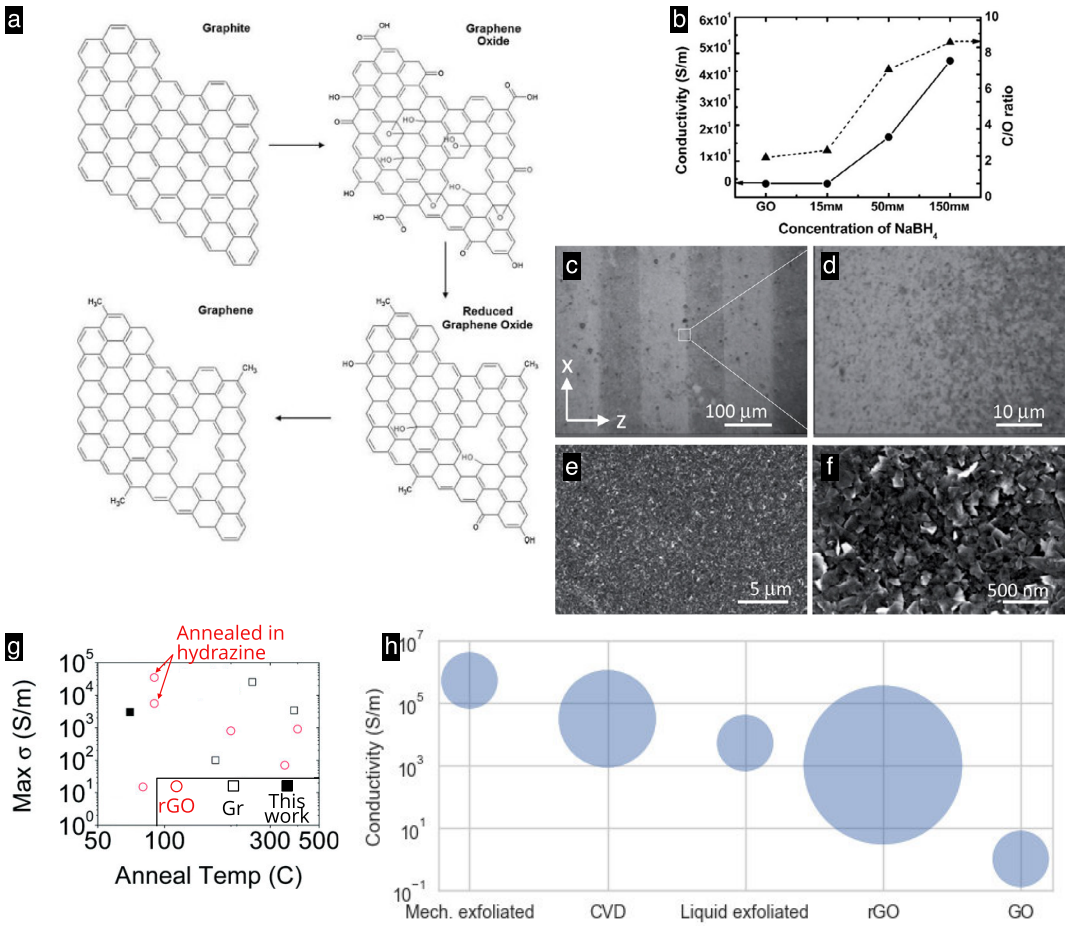

Figure 1. (a) Chemical structures of graphite, graphene oxide, reduced graphene oxide and graphene as described by Mohan *et al* [28], copyright 2015, with permission from Elsevier. (b) Reducing graphene oxide (GO) in $NaBH_4$ decreases its oxygen content and increases its conductivity (adapted from [32], John Wiley & Sons, copyright 2009 WILEY-VCH Verlag GmbH & Co. KGaA, Weinheim). (c) and (d) Optical images of inkjet-printed liquid-exfoliated graphene, and (e) and (f) SEM images of the film morphology. (g) Inkjet printing liquid-exfoliated graphene offers good conductivities without aggressive treatments (adapted from [33] with permission of The Royal Society of Chemistry). (h) The measured conductivities of the available graphene sources. Exfoliated material possesses the highest conductivities but production challenges limit its application; materials produced by each of the other methods are more readily produced.

There is a strong relationship between the structure of rGO and its electrical conductivity. Mohan *et al* [28] reported the synthesis and subsequent reduction of GO in order to maximize the electrical conductivity. They reported an electrical conductivity as high as 10^3 S m^{-1} for an rGO film reduced with hydroiodic acid (HI). Furthermore, Shin *et al* [32] demonstrated that the conductivity of graphite oxide films could be modulated using reducing agents (such as sodium borohydride, $NaBH_4$) and they elucidated the underlying reduction mechanism. This involved the formation of boron oxides that were subsequently removed at higher concentrations. They found that increasing the concentration of $NaBH_4$ led to higher C/O ratios and subsequently to higher electrical conductivities, as shown in figure 1(b). Using $NaBH_4$ instead of hydrazine to reduce GO is advantageous because, during hydrazine reduction, nitrogen-containing functional groups can form, whose presence then leads to an increase in sheet resistance [32].

Thermal treatments have also been applied, and generally perform better at recovering conductivity compared to chemical treatments. Thin films of rGO (∼10 nm thick) displayed increasing conductivities from 3 S m^{-1} to 10×10^4 S m^{-1} by tuning the annealing temperature (T_{ann}) from 200 °C to 940 °C [40]. Becerril *et al* obtained conductivities of $\sim 5 \times 10^4$ S m^{-1} after being heated to 1100 ° C whilst still maintaining 80% transmittance [41]. As a comparison, the same study found a hydrazine treatment followed by annealing at 400 °C gave $\sim 5 \times 10^3$ S m^{-1} with a similar transmittance. More recently, thin films of rGO have reached 9×10^4 S m^{-1}, after annealing at 1000 °C in a Ar/H_2 atmosphere [42]. By annealing at even higher temperatures (>2000 °C) using arc discharge it is possible to recover conductivities of 2×10^5 S m^{-1} [43], with the downside here of scalability.

Despite some success, these reduction methods have not been able to recover the pristine conductivity of graphene. Even the complete removal of oxygen groups does not fully recover the properties of pristine graphene as defects in the lattice remain. Therefore, only isolated conductive regions of graphene are recovered, and electrons are required to hop between

these neighbouring regions, reducing the conductivity [36]. For this reason, covalently functionalised graphene may not be a suitable material for high-end electrical applications, and flakes that remain unmodified are likely to be more advantageous [44].

2.4. Liquid exfoliation

It is possible to exfoliate graphite in liquid without heavily functionalising the graphene sheets. Paton *et al* produced exfoliated graphene in a liquid using surfactants to stabilise the graphene sheets [45]. Flakes typically 1–10 layers in thickness and with lateral dimensions of 500–1000 nm were produced [5, 46]. This route yielded large volumes of high-quality graphene that was solution-processable and with few defects. The presence of surfactant, however, can decrease the conductivity of the films [47]. More recently, inkjet-printed thin-films of liquid exfoliated graphene were reported. The graphene was printed repeatedly to form films of different thickness, as shown in the optical microscope images in figures 1(c) and (d). SEM images (figures 1(e) and (f)) reveal that the flakes were randomly orientated within the film. Repeated printings of the graphene flakes increased the film's conductivity, and the maximum recorded conductivity was 3000 S m^{-1} [33]. This value is relatively high compared to other solution-processable techniques, as shown in figure 1(g), and also avoids the use of harsh chemicals and high temperatures.

2.5. Graphene nanoplatelets

Another promising candidate for composites is graphene (or graphite) nanoplatelets (GNPs), which are typically much cheaper than other forms of graphene, and are commercially available on the tonne scale. Production methods vary, but most exfoliate bulk graphite using thermal expansion, or mechanical agitation, or both. The dimensions, primarily the thickness, of GNPs dictate their intrinsic conductivity, with thinner GNPs having the highest values: GNPs with thickness of 50 nm, 5 nm and 3 nm have conductivities of 7×10^4 S m^{-1}, 1×10^5 S m^{-1} and 1.5×10^5 S m^{-1} respectively [48]. The reason for this thickness effect is thought to be the poor c-plane conductivity of graphite. Thus producing thin flakes (<10 layers) remains a priority for the preparation of conductive graphene-based composites.

In summary, the conductivity of graphene materials produced using different synthetic routes spans almost 8 orders of magnitude: from the poor conductivity of heavily functionalised graphene oxide (10^{-2} S m^{-1}) to the exceptional conductivity of graphene produced by mechanical exfoliation (10^6 S m^{-1}). These values are summarised in figure 1(h). However, for practical applications such as polymer nanocomposites, there is a balance of quality against the ability to produce the material on the required scale. So while mechanically exfoliated and CVD graphene have the advantage of high conductivities, they are unlikely to have the production capacity to meet the demands of composites. GO can overcome this disadvantage because it has a solution-processable, scalable production route. However, the oxygen containing functionalities decrease the conductivity of the graphene. This has been overcome to a certain extent with reduction methods, but pristine graphene is yet to be recovered. Liquid exfoliated graphene and GNPs remain mostly unfunctionalised and so do not suffer the same quality degradation, and also have the advantage of scalable production routes. For these reasons, they show the most promise for conductive polymer composites.

3. Fundamental aspects of electrical conductivity in composites

3.1. Percolation theory

The versatility of polymers make them attractive for many applications but they are generally unsuitable for conducting applications because most polymers are insulating. Conductive composites can be achieved by adding a conductive filler to the polymer matrix. For a random distribution of this filler, a conducting network will form at a specific loading, known as the percolation threshold (p_c). When the filler loading reaches p_c, the conductivity of the composite rises suddenly and the graph of conductivity versus loading takes the characteristic S-shape, demonstrating the three characteristic regimes: insulating, percolating and conductive (shown in figure 2(a)).

The conductive behaviour in these three regimes can be understood from the microstructure of the composite. When there is no conductive path through the filler, no charge can flow, and the composite remains insulating. On the other hand, if the filler forms a directly connected network, electrons can move through this network, and the composite is conductive. Between these two extremes, conduction takes place when the fillers are not in direct contact but are connected via electrons tunnelling through an interface formed between the filler and the matrix; the conductivity in this case is lower than that where a direct network has been formed. This tunnelling conduction is a quantum phenomenon where the contribution between the nearest neighbours is the most dominant [49–52]. Tunnelling transport has been directly observed in a carbon-nanofiber polymer composite using conductive-tip atomic force microscopy [53].

The percolation properties can also be affected when the filler forms aggregated structures that are then interconnected by individual filler particles. Often this agglomeration can promote percolation. In a similar vein, the fillers can form a phase-separated, co-continuous morphology comprising of graphene-rich and -poor phases within the volume of the composite. This is known as selective localization [54, 55] and often leads to a conductive composite at lower loadings.

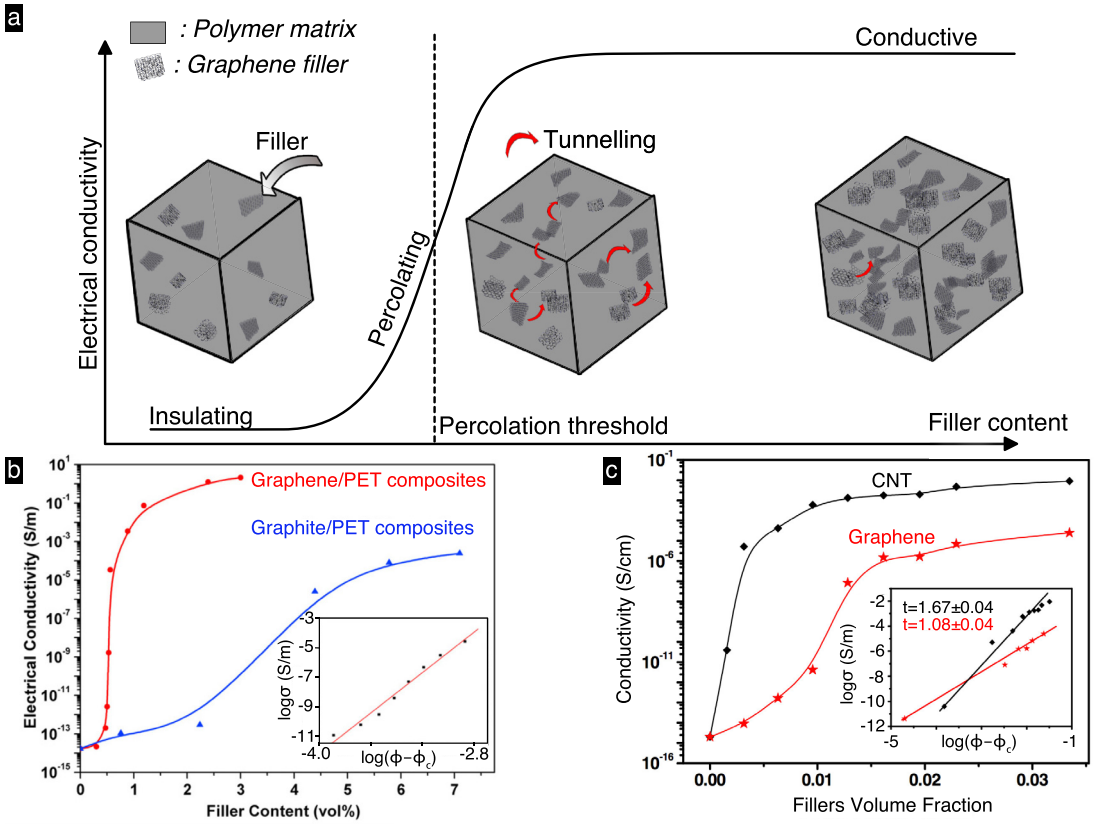

Figure 2. (a) A schematic of conduction mechanisms in a composite with increasing filler content. At no loading, the polymer is insulating, and remains insulating while the loadings are low. As the filler content is increased to the percolation threshold, a conductive network begins to form. At loadings greater than this, an efficient network has been formed and the conductivity is saturated. (b) Graphene enables a significantly lower percolation threshold in PET than graphite (adapted from [56], copyright 2010, with permission from Elsevier). (c) An example of the percolation threshold in high density polyethylene (HDPE) composites formed with CNT (black) and graphene nanosheets (red) (adapted from [57], copyright 2011, with permission from Elsevier).

Both simulations and experiments have shown that fillers with larger aspect ratios lead to reduced percolation thresholds (the modelling of this effect is discussed further in section 3.2) [58, 59]. Thus, graphene is one of the most efficient fillers available due to its large aspect ratio. For example, Zhang *et al* filled PET with graphene and graphite and measured the percolation threshold for each filler [56]. The threshold for graphene (0.47 vol%) was significantly lower than that measured for graphite (∼4 vol%), as shown in figure 2(b). These experimental results were supported by simulations performed by Ambrosetti *et al*, who found that conductive, platelike objects with an aspect ratio of 100 yielded a composite with a percolation threshold 26 times lower than those formed with objects of aspect ratio 1 [58].

This ideal behaviour caused by high-aspect-ratio fillers can, however, be strongly affected by the preparation method. For example, Du *et al* [57] prepared high density polyethylene nanocomposites with graphene nanosheets (GNSs) and carbon nanotubes. They found that the samples filled with CNTs had a lower percolation threshold than those with GNSs (as shown in figure 2(c)), because the GNSs tended to aggregate and wrinkle, reducing their effective aspect ratio, and hindering the network formation. In fact, an ultra-low percolation threshold was achieved with CNTs (0.0025 vol%) because their high aspect ratio was maintained. On the other hand, graphene has the advantage of easier processability compared to CNTs as the viscosity of graphene composites is significantly lower than CNT-ones at the same loadings [10]. This means that a greater amount of filler can be introduced in the matrix, leading to higher ultimate values of conductivity.

Several theories have been developed for the evaluation of the effect of the number of interconnections on the conductivity of a random system but the number of variables affecting the conductivity of these systems makes the task challenging. Fournier *et al* used an analytical model which is based on the Fermi–Dirac distribution for the study of the transition from insulator to conductor [60]. In this case the conductivity is given by:

$$log(\sigma_c) = \log(\sigma_{gr}) + \frac{\log(\sigma_m) - \log(\sigma_{gr})}{1 + e^{b(p-p_c)}} \quad (1)$$

where σ_c, σ_{gr}, σ_m, are the conductivities of the composite, graphene and matrix respectively, p is the mass fraction, p_c is the percolation threshold and b is an empirical parameter that leads to the change in electrical conductivity at p_c. A fit of this equation against the experimental data will determine the percolation threshold.

The majority of reports in the literature use the classical percolation theory [61] in order to model the conductivity of composites. The equation that describes this theory is:

$$\sigma_c = \sigma_{gr}(\psi_{gr} - \psi_c)^t \quad (2)$$

where ψ_{gr} is the volume fraction of graphene and ψ_c is the percolation volume fraction, while σ_c and σ_{gr} are the conductivity of the composite and the graphene respectively. Moreover, t is the critical power law exponent and depends on the dimensionality of the network, normally taking values of ~1.33 for 2D systems [62] (such as when confined in a coating) and ~2 for 3D systems [63].

3.2. Modelling percolation in graphene composites

To model the electrically percolating behaviour in composites, one common approach is to use Monte Carlo methods. Here the fillers are represented by geometric objects that are placed randomly inside a constrained volume that represents the matrix. Once the objects are placed, the junctions between them are identified, and their junction resistance, R_J is calculated. This is often done using the formula derived by Simmons [64]:

$$R_J = \frac{V}{A_J J_0 \left(\psi_1 e^{-K\sqrt{\psi_1}} - (\psi_1 + eV)e^{-K\sqrt{\psi_1 + eV}}\right)} \quad (3)$$

where V is the voltage across the junction, A_J the contact area of the junction, J_0 an arbitrary constant, and e the charge on an electron. The constant $K = 4\pi\Delta s\sqrt{2m}/h$ is a combination of Planck's constant h, the mass of an electron m, and the limits of the barrier at the Fermi level Δs. Finally, ψ_1 is the mean tunnel barrier height and depends on the filler work function and the dielectric constant of the insulating matrix.

The representation of the filler is a key component of these methods. A common approach is the 'hard core, soft shell' structure. The hard core takes the dimensions of the physical graphene sheet, and the soft shell extends a few nanometres around the core to represent the tunnelling distance of the electrons. The cores cannot penetrate each other, but core and shells can overlap. When they do, a tunnelling junction is formed. These methods successfully modelled percolation thresholds in composites of graphene [65], and have also been applied to other nanofillers, such as CNTs [66]. In these models, the junction resistance is much larger than the resistance of the filler, and so the filler resistance is often ignored. This is particularly true for highly conductive fillers such as pristine graphene and CNTs. However, how the resistance of a less conductive filler, such as GO, could affect the overall network resistance has been less comprehensively studied.

These models also give insight into the ideal physical properties for the graphene filler. Hicks *et al* investigated the effect of filler aspect ratio on the conductivity of the resulting composite [65]. They found that large aspect ratios lead to a higher conductivity. This was particularly important at lower filler contents. This was because fillers with large aspect ratios form a network with fewer junctions than those with smaller aspect ratios, and fewer junctions reduces the total resistance of the network. In a similar way Zabihi *et al* found that fillers formed of larger sheets gave composites with higher conductivities [67].

It is also possible to predict the ideal dispersion of the filler. For example, models have shown that agglomeration of the filler will lead to lower percolation thresholds [68]. This result has been experimentally validated by using selective localisation, where the filler can be confined to only one of multiple matrices. This agglomeration effect is less important at higher loadings, where the probability of forming a conductive network is much higher. Another example is the alignment of the filler within the composite. Zabihi *et al* found that the flake-normal should be perpendicular to the electric field when the filler is disc-like [67]. This is to maximise the probability of forming a conductive network inside the composite.

Extensions to the model outlined above have helped understand other results from electrical composites, like the percolation of charge under alternating current (AC). Hashemi *et al* effectively modelled the response of a composite to AC current by including microcapacitors within the composite [69]. These microcapacitors represent fillers that are isolated by a thin layer of matrix, where charge can accumulate. Even better agreement (particularly at higher frequencies) was found by including frequency-affected tunnelling and Debye dielectric relaxation into the model, along with the microcapacitors [70]. Further developments on the temperature behaviour of composites have been made; in some cases, heating the composite causes the polymer to expand, which consolidates the conductive network, and so increases the composite's conductivity [71].

3.3. Conduction mechanisms in disordered graphene sheets

Different conduction mechanisms are observed when there is disorder in an insulator-conductor composite. Often charge will percolate via a hopping conduction mechanism [72], which involves the excitation of charge carriers into free, delocalised states [73]. Electrons then hop between the available states to transport charge. Hopping conduction mechanisms are split into two main mechanisms: nearest neighbour hopping and variable range hopping (VRH). Both mechanisms normally proceed simultaneously, but usually one is dominant. The general equation for hopping conduction is [74]:

$$\sigma(T) = \sigma_0 e^{-\left(\frac{T_0}{T}\right)^\gamma} \quad (4)$$

where T is temperature, σ_0 and T_0 are constants (although they do have some T dependence, it

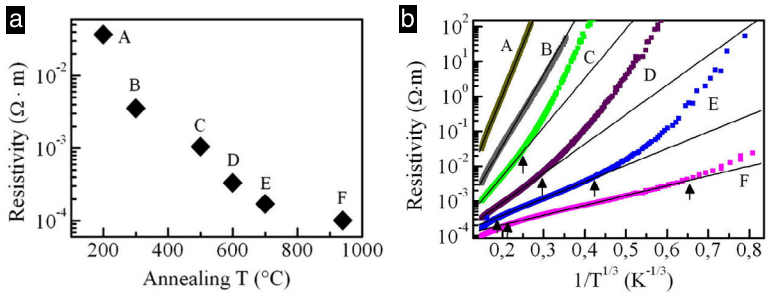

Figure 3. (a) Room temperature electrical resistivity of the rGO films prepared with different annealing temperatures. (b) Electrical resistivity versus $(1/T)^{1/3}$ for different annealing temperatures as denoted by the letter, which corresponds to the films in (a). The arrows denote the transition temperature from the VHR regime. Black lines indicate the 2D-Mott VHR model.

has a much weaker effect), and γ is the hopping exponent. The hopping exponent depends on the dominant hopping mechanism, which itself depends on the temperature of the system. At low temperatures variable range hopping is dominant. The hopping exponent then depends on the available dimensions of the hopping as $\gamma = 1/(D+1)$ where D is the dimensionality. For 3D systems then, the equation yields:

$$\sigma(T) = \sigma_0 e^{-\left(\frac{T_0}{T}\right)^{\frac{1}{4}}} \quad (5)$$

which is the same formalism as derived by Mott [75].

Mott VRH theory considers the density of states (DOS) as a constant value. However, the promotion of one electron to the unfilled state creates a hole in the occupied site. This electron-hole pair system modifies the DOS which vanishes at the Fermi energy due to long-range Coulomb interactions. This model is called Efros and Shklovskii (ES-VRH) and is described by a charge transport equation similar to the Mott model, where the exponent γ does not depend on system dimensions and is equal to 1/2.

While the electron transport properties of the single layer are studied in detail (e.g. ES-VRH model well describes the behaviour of rGO [76]), the conduction mechanisms involved in disordered graphene sheets are still not well established. In general, such systems are continuous thin films corresponding to a non-percolative regime, which can be described as a dense mesh.

rGO thin films can be used as an ideal test-bed system to understand the charge transport mechanisms in partially disordered systems; in the film, the single rGO sheets are placed all parallel to each other, and stacked together. This film yields a highly anisotropic conductive system, where the electric resistance at junctions between neighbouring sheets depends on the sheets stacking and overlap. The building block of such materials are single GO sheets which, due to their excellent processability in solution, can assemble in uniform and continuous thin (~10 nm) films on large scale (tens of cm^2). Once fixed, the morphology of the thin film (i.e. position, number and shape of single sheets), the role of the structural order (i.e. amount of sp^2 regions and defects) and its relationship with the charge transport can be systematically studied by performing several reduction levels in a controllable way.

Vianelli *et al* [40] investigated the temperature dependence of charge transport properties of rGO thin films, tuning the sheet conductivity and number of defects by thermal reduction before the measurement (figure 3(a)). They characterized the electrical transport properties at intermediate reduction stages and in a wide temperature range (2–300 K), wide enough to assess the validity of different charge transport models.

The temperature dependence of the resistance $R(T)$, as depicted in figure 3(b), fits well with equation (4) below the liquid nitrogen temperature, consistently with 2D-VRH model ($\gamma = 1/3$). At lower temperatures, a crossover to another regime, still to be identified, likely occurs. Hopping presumably occurs between the sp^2 regions by consecutive inelastic tunnelling processes. The scaling of the slope of the $R(T)$ curves with increasing T_{ann}, clearly indicates a gain in the electrical conductivity due to the restoration of $\pi - \pi$ bonds and the decrease of the number of defects.

For a high degree of reduction of rGO ($T_{ann} = 700$ °C and 940 °C), deviations are observed at high temperatures (T > 100 °C), ascribed to a crossover to an Arrhenius-like regime ($\gamma = 1$), where 3D thermally activated processes start to dominate the conduction.

4. Graphene-based composites

4.1. Ideal composites

An ideal graphene-based composite system would comprise continuous graphene sheets with a large lateral size, that could be well dispersed within the matrix. CVD offers this as it produces high-quality graphene with large lateral dimensions. Vlassiouk *et al* [77] prepared composites of poly(methyl methacrylate) (PMMA) and CVD graphene using a layer-by-layer approach. As shown in figure 4(a), they formed two structures: a flat laminate (type 1) and a rolled scroll to form a fibre (type 2). The graphene loading in the flat laminate composite was only 0.13 vol%, however the conductivity was among the

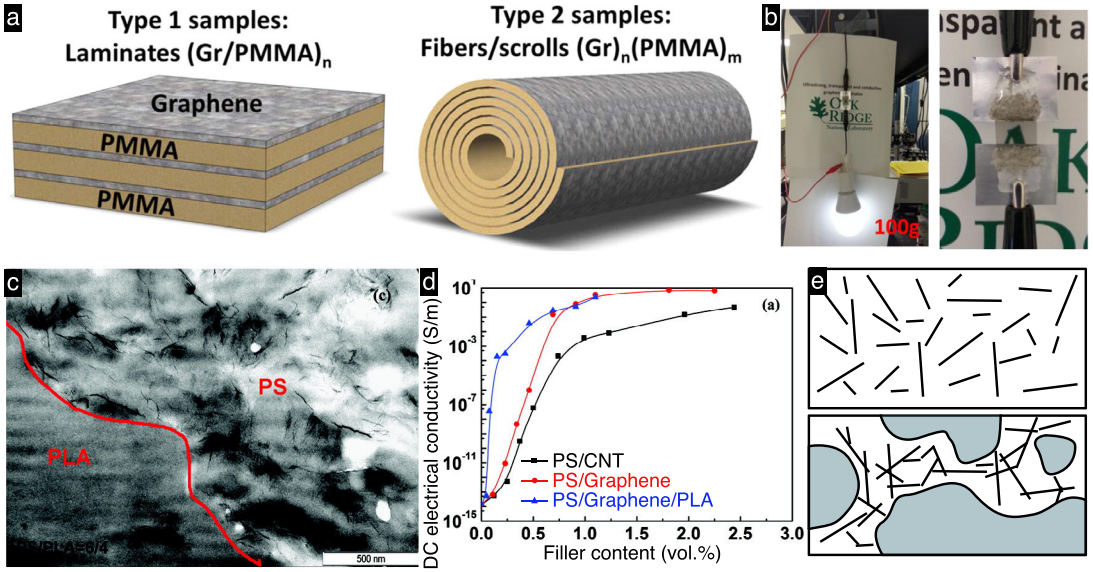

Figure 4. (a) Ideal composites made from CVD-graphene and PMMA layers that can either be flat or rolled into scrolls. (b) These composites are strong and conductive (adapted from [77], copyright 2015 American Chemical Society). (c) TEM image of PS/PLA (60:40) composite with 0.46 vol% graphene. The selective localization of graphene can be seen, and this results in a lower percolation threshold (d) (adapted from [79], copyright 2011 American Chemical Society). (e) Selective localisation forces the graphene into a smaller volume so a conductive pathway can be formed at lower filler contents (adapted from [54], copyright 2011, with permission from Elsevier).

highest reported for graphene-based nanocomposites, at 810 S m^{-1}. This is a result of the ideal composite architecture of perfectly oriented graphene layers with no crumpling or rolling of the graphene. These composites were strong enough and conductive enough to support and provide power to a light bulb, as shown in figure 4(b). Liu *et al* subsequently prepared similar polycarbonate/CVD-graphene layered composites with a conductivity of 420 S m^{-1} at a filler content of 0.19 vol%, while the percolation threshold was as low as 0.003 vol% [78]. This is a highly-promising procedure for the production of advanced, multifunctional graphene-based nanocomposites, however producing these materials in bulk quantities is still challenging. A summary of the properties of these composites, and those discussed later, is presented in table 1.

4.2. Graphene nanoplatelets

Graphene nanoplatelets (GNPs) are among the most popular materials used for filling polymer matrices because of their inherent tensile strength, electrical and thermal conductivity, and their availability in bulk quantities. However, for GNPs, the composite preparation method is particularly important as they are prone to crumple, wrinkle, and roll during processing. This is particularly important for high-shear processes such as melt mixing. In contrast, using solution blending can preserve the original form of the GNPs. An additional benefit of solution blending is that the viscosity of the nanocomposite is lower than those prepared by melt mixing, which allows the macromolecular chains to intercalate between the graphite layers during the preparation process [80]. As an example, Pang *et al* [81] used a solvent-assisted dispersion method followed by hot compression during the production of UHMWPE/GNP composites and they achieved a very low percolation threshold at only 0.07 vol% filler content. Other preparation methods have the advantage of distributing the flakes uniformly through the matrix, as exampled by *in situ* polymerization.

Kim *et al* conducted a comparison of the different effect of processing methods (solution blending, *in situ* polymerization, and melt compounding) on the conductivity of polyurethane/graphene nanocomposites [82]. They found that the highest conductivity values were obtained from composites prepared via solution blending: melt mixing lead to particle re-aggregation and particle attrition that reduced the lateral size of the graphene; and *in situ* polymerization caused covalent bonds to form between the matrix and the filler, which hindered direct contact between the fillers and reduced the effective aspect ratio. Similar results were also reported in the works of Kim *et al* [54] and Xu *et al* [83]. For all production methods, post-processing methods such as hot pressing or injection moulding can further affect the dispersion of the fillers and the ultimate conductivity of the composite.

The alignment of the filler within the matrix can also be affected by the processing conditions. The most industrially relevant preparation method is extrusion, and different types of extrusion can cause different orientation characteristics in the final composite. For example, the use of small-scale extrusion [84–88] and mono extrusion [89] have both been shown to cause a random orientation of GNPs within the polymer. On the other hand, multilayer coextrusion [89, 90] and

blown film extrusion [91, 92] can give composites with orientated GNP flakes. Extrusion is very commonly followed by other processing steps, such as injection moulding or melt-mixing, in order to formulate the samples into well-defined specimens for testing, so post-processing can always alter the morphology of the flakes after extrusion [80, 93–95]. Therefore, there are other more reliable strategies for forcing the fillers to align, and these are discussed further in section 4.4.

Under the correct processing conditions, the selective-localization principle may also influence the conductivity of GNP-based composites. In this case, graphene is predominantly present in specific parts of the composite (often in distinct matrices), reducing the percolation threshold for the overall material. Qi *et al* prepared conductive graphene/polystyrene composites by solution mixing and reached percolation at a graphene content of 0.33 vol% [79] (figure 4(c)). These graphene composites had ultimate conductivity values of 2–4 orders of magnitude higher than those with CNTs produced in the same way. Qi *et al* then produced polymer blends where poly(lactic acid) (PLA) was incorporated in the graphene/PS composite. Graphene was found in these blended systems to localize in the PS-rich regions, resulting in a reduced percolation threshold of 0.075 vol%. Figure 4(e) shows schematically how selective localisation lowers the percolation threshold. When material is uniformly distributed, it cannot form a conductive network; if, however, the same amount of material is localised in a smaller volume, a network is more likely formed.

Moreover, functionalisation of the filler can help towards the improvement of solubility and processability, enhancing the interactions between the filler and the matrix, enabling a more homogeneous dispersion. However, the covalent interactions between the fillers and the matrix can sometimes disrupt the sp^2 hybridized carbon atom conductive pathways and reduce the electrical conductivity [96, 97].

4.3. Graphene oxide and reduced derivatives

GO has a relatively low conductivity, but the functional groups on the graphene sheets can provide some advantages when used in composites. Most significantly, they can alter the van der Waals interactions between the GO and the matrix, leading to a better dispersion of the GO sheets within the polymers [29, 41, 98–101]. For this reason, GO has attracted considerable attention as a nanofiller for polymer nanocomposites. The electrically insulating nature can be reversed to give a material more akin to graphene through either thermal or chemical reduction. A wide range of conductivities and percolation thresholds of GO and reduced GO composites depending on the processing method, polymer matrix and filler type have been reported. The electrical performance of both thermally reduced GO (TRGO)- and chemically reduced GO (CRGO)-based polymer nanocomposites are discussed in the next sections.

4.3.1. Thermally reduced GO (TRGO) based composites

Thermally reduced graphene oxide (TRGO) has been obtained by oxidation of graphite followed by thermal expansion [102], which increases the carbon percentage of the GO materials up to 97 wt.%, and increases their conductivity up to $\sim 10^5$ S m^{-1}.

The presence of the remaining functional groups after the thermal treatment still promotes dispersion and interfacial adhesion in many polymer matrices. This makes TRGO a very promising nanomaterial to blend with polar polymers [54, 82, 102–112]. Several groups have employed TRGO materials to prepare thermoplastic nanocomposites from polyethylene [54, 113], maleic-anhydride grafted poly(propylene) [114], polystyrene [115] and ethylene/methyl acrylate/acrylic acid copolymers [116], as well as poly(methyl metacrylate) (PMMA) [106] and TPU [82] .

The use of TRGO to enhance the electrical performance of polymers has been successfully demonstrated for thermoplastics. Steurer *et al* melt compounded isotactic poly(propylene) (iPP), poly(styrene-co-acrylonitrile) (SAN), polyamide 6 (PA6), and polycarbonate (PC) in a twin-screw mini-extruder together with TRGO [102]. They showed that TRGO with aspect ratios >200 can be uniformly dispersed during melt extrusion. As shown in figure 5(a), the authors observed electrical percolation at 4 wt.% TRGO loading into SAN, which gave a conductivity of 3.7×10^{-8} S m^{-1} (as a comparison, at the same content of CB the conductivity was much lower, $\approx 10^{-13}$ S m^{-1}). By adding 12 wt.% of TRGO a specific conductivity of 2 S m^{-1} was measured, the same as that of the pure filler. For PC they measured a lower percolation threshold at a loading of 2.5 wt.% and yielding a conductivity of 7.7×10^{-6} S m^{-1}.

In addition to thermoplastics, elastomers have also recently been combined with GO materials. For example, natural rubber (NR) latex nanocomposites have been reinforced with TRGO materials, and show electrical percolation at 3 phr, with measured conductivities around 10^{-4} S m^{-1} [107]. In addition, a study on styrene-butadiene rubber (SBR) [103] has recently shown that TRGO exhibits superior electrical performance with respect to other carbon nanofillers such as carbon black, expanded graphite, and carbon nanotubes. The TRGO/SBR composite maintained good conductivity even at low electrical frequency, as shown in figure 5(b). Other groups have also found enhanced electrical conductivity in SBR/TRGO composites [117], and in natural rubber composites [118, 119].

In all these cases, TRGO efficiently forms a percolated network. TRGO composites showed lower percolation thresholds than those containing CNTs, which was attributed to the higher aspect ratio of TRGO compared to 0D or 1D carbon nanoparticles [102, 104]. This low percolation threshold is useful when producing nanocomposites with a low filler content. However, the maximum conductivity achieved

Table 1. A summary of the conductive properties of graphene polymer nanocomposites, based on the graphene production method and the polymer processing method. Composites with CNT and CB fillers are included where the studies made direct comparisons.

Polymer matrix	Filler	Preparation method	Percolation threshold	Ultimate DC conductivity (S m^{-1})	Reference
ABS	GO	Coagulation blending	0.13 vol%	0.1	[168]
PA6	TRGO	Melt compounding	7.5 wt.%	7.1×10^{-3}	[102]
	CB		7.5 wt.%	2.2×10^{-8}	
	CNT		—	—	
PA6	rGO	*In situ* polymerization	0.41 vol%	0.028	[169]
PA11	GNP	Masterbatch extrusion	0.25 vol%	5.2×10^{-6}	[170]
PA12	TRGO	Melt compounding	1–2.5 wt.%	5.2×10^{-6}	[109]
	N-TRGO		1 wt.%	10^{-4}	
PA12	TRGO	Melt compounding	2.5 wt.%	8.9×10^{-2}	[112]
	MLG 350		2.5 wt.%	1.2×10^{-2}	
	EG		10 wt.%	6.6×10^{-8}	
	CNTs		5 wt.%	0.16	
	CB		5 wt.%	0.13	
PC	TRGO	Melt compounding	2.5 wt.%	0.1	[102]
	CB		2.5 wt.%	9.1	
	CNT		2.5 wt.%	0.56	
PC	rGO	Solution blending/ *In situ* thermal reduction	0.21	0.1	[171]
PC	f-GNP	Emulsion mixing	0.14 vol%	51	[172]
POSS-PCL	rGO	Solution blending	2.5 vol%	0.1	[173]
PE	f-GNP	Melt mixing	0.83 vol%	0.01	[174]
LLDPE	TRGO	Melt mixing	0.5 vol%	10^{-4}	[104]
LLDPE	TRGO	Melt compounding	0.5–0.9 vol.%	10^{-4}	[104]
HDPE	f-GNP	Solution blending	0.37–0.74 vol%	27	[175]
UHMWPE	rGO	Solution blending and hydrazine reduction	0.028 vol%	5	[176]
PLA	GNP	Solution blending	0.004 vol%	0.1	[177]
PLA	TRGO	*In situ* polymerization	0.5–0.75 vol%	0.01	[178]
PMMA	rGO	Solution blending	0.25 vol%	0.01	[179]
P(MMA-co-BA)	GNP	Latex blending	0.1 vol%	217	[180]
PMMA	f-GNP	Solution blending	0.3	10^{-3}	[181]
PMMA	f-TRG	Self-assembly	0.06 vol%	1.2	[182]
PMMA	f-GNP	Solution blending	0.8 vol%	20	[106]
iPP	TRGO	Melt compounding	5 wt.%	5.3×10^{-2}	[102]
	CB		5 wt.%	3.3	
	CNT		5 wt.%	3.1	
TPU/PP	f-rGO	Solution-flocculation and melt mixing	0.054 vol%	10^{-6}	[183]
PP	TRGO	Melt compounding	<5 wt.%	10^{-4}	[110]
	MLG		5 wt.%	3×10^{-3}	
	CB		7.5 wt.%	3×10^{-5}	
	CNT		7.5 wt.%	4×10^{-6}	
	EG		—	—	
PS	CRGO	Solution mixing + freeze-drying	<1 wt.%	15	[127]
PS	rGO	LbL assembly	0.2 vol.% (1 layer)	0.05	[129]

(*Continued*)

Table 1. (*Continued*)

Polymer matrix	Filler	Preparation method	Percolation threshold	Ultimate DC conductivity (S m^{-1})	Reference
PS	GNP	Solution blending	0.1 vol%	13.8	[184]
PS	GNP	Solution blending	0.33 vol%	3.5	[79]
PS/PLA			0.075 vol%	3	
PS	GNP	Electrostatic self-assembly	0.09 vol%	25	[185]
sPS	GNP	Solution blending	0.46 vol%	470	[186]
PS	GNP	Electrostatic assembly	0.054 vol%	46	[187]
PU	f-TRGO	*In situ* polymerization	0.5–2 wt.%	1.4×10^{-7}	[111]
	CB		2 wt.%	1.3×10^{-7}	
	CNT		2 wt.%	1.9×10^{-7}	
PU	rGO	Solution blending	0.078 vol%	0.001	[149]
PVC	GNP	Solution blending	0.1 vol%	5.8	[188]
SAN	TRGO	Melt compounding	4 wt.%	0.123	[102]
	CB		4 wt.%	9	
	CNT		12 wt.%	7.4×10^{-4}	
Epoxy	f-GNP	Solution blending	1.3 vol%	10^{-6}	[189]
Epoxy	f-rGO	Solution blending	0.71 vol%	10^{-6}	[190]
Epoxy	f-GNP	Sonication/Calendaring	4 vol%	10^{-4}	[191]
Epoxy	GNP	Solution blending	0.5–1 vol%	10^{-2}	[192]
Epoxy	GNP	Layer by Layer	0.6 vol%	10^{-4}	[193]
Epoxy	CRGO	*In situ* polimerization	0.12 vol.%	0.1	[128]
Epoxy	CRGO aerogel	Vacuum-assisted infiltration method	<0.25 wt.%	20	[147]
Epoxy	TRGO	Solvent free mixing method	1 wt.%	2×10^{-6}	[105]
	N-TRGO		1 wt.%	10^{-5}	
	DMG		5 wt.%	8×10^{-5}	
Epoxy	GNP	Solution blending	0.52 vol%	0.05	[194]
Epoxy	f-GNP	Solution blending	0.16 vol%	10	[195]
Epoxy	rGO		0.12 vol%	1	[150]
Epoxy	GNP	Three roll mill	0.22 vol%	10^{-5}	[146]
Epoxy	f-GO	Solution blending	0.78 vol%	1	[196]
PI	f-GNP	*In situ* polymerization	0.5 vol%	0.1	[197]
PI	f-GO	*In situ* polymerization	0.25 vol%	0.092	[198]
NR	GNP	Latex self-assembly	0.62 vol%	0.03	[132]
NR	CRGO	Coagulation method	3 wt.%	10^{-4}	[118]
NR	TEGO	Two-roll mill	0.02 vol.%	3.4×10^{-9}	[119]
NR	f-rGO	Electrostatic self-assembly	0.21	7.3	[199]
NR	rGO	Vacuum-assisted self-assembly	10 phr	100	[200]
NR	TRGO	Latex technologically	3 phr	10^{-4}	[107]
NR	rGO	Electrostatic self-assembly	0.23	1	[201]
NR	rGO	Solution blending	0.21 vol%	0.23	[202]
SBR	Surface-modified MLGs	Hetero-coagulation method	0.5 wt.%	8.2×10^{-4}	[117]
SBR	f-3D-GO	Latex coagulation	0.39 vol%	10^{-2}	[203]
XNBR	TRGO	Electrostatic LbL self-assembly	—	0.82	[108]

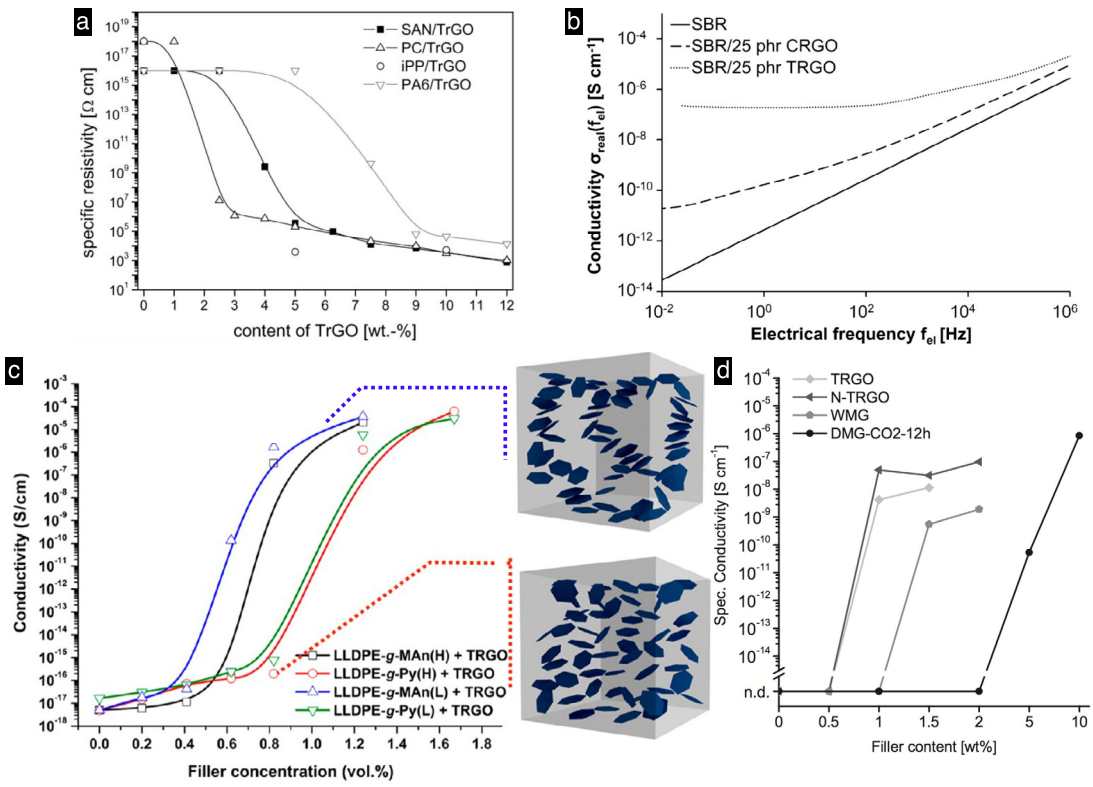

Figure 5. (a) Specific resistivity of SAN, PC, iPP and PA6 nanocomposites as a function of the TRGO content (adapted from [102], John Wiley & Sons, copyright 2009 WILEY-VCH Verlag GmbH & Co. KGaA, Weinheim). (b) The conductivity of SBR composites as a function of electrical frequency (adapted from [103], John Wiley & Sons, copyright 2009 WILEY-VCH Verlag GmbH & Co. KGaA, Weinheim). (c) Chemically compatibilised composites show a reduced percolation threshold because the graphene filler forms a conductive path more readily (adapted from [104], copyright 2014 American Chemical Society). The filler forms a stronger network through aggregation for LLDPE-g-MAn as shown schematically. For LLDPE-g-Py the same aggregation is not observed and the resulting percolation threshold is higher. (d) Nitrogen-doped TRGO yields a slightly higher conductivity (and slightly lower percolation threshold) than TRGO without nitrogen doping (adapted from [105], John Wiley & Sons, copyright 2009 WILEY-VCH Verlag GmbH & Co. KGaA, Weinheim).

with TRGO materials is about ten times lower than that of the equivalent CNT-based composites. This is likely due to the residual oxygen in TRGO, and the presence of defects, that both reduce its conductivity. This shows a key limitation of using functionalised graphene as a conductive filler.

Chemical compatibilisation can improve the interfacial adhesion between the filler TRGO and the polymer: better adhesion leads to a better dispersion and results in a lower electrical percolation threshold. An example is the work reported by Shim *et al*, who coagulated SBR together with raw, carboxylated, and cetyltrimethylammonium bromide stabilized TRGO, and reported improvements on the electrical conductivity, showing percolation thresholds as low as 0.5 wt.% [117, 120]. Another example is the addition of TRGO to maleated linear low-density polyethylene (LLDPE) and to its derivatives with pyridine aromatic groups by melt compounding [104]. In this report, low electrical percolation thresholds of between 0.5 and 0.9 vol.% were found [104] (as shown in figure 5(c)). However, preparing nanocomposites by melt mixing is difficult due to the low density and very high surface area of TRGO. Further, TRGO often requires special handling and safety procedures. An alternative to thermal reduction of GO is the chemical reduction of GO materials.

4.3.2. Chemically reduced GO (CRGO) based composites

Chemically reduced aqueous GO dispersions can be produced by exposing GO to strong reducing agents such as hydrazine. These treatments are not able to completely remove oxygen from the graphene sheets: the oxygen content of CRGO materials is similar to that of TRGO produced at 400 °C (≈15% oxygen). Agglomeration, where the graphene sheets restack after reduction, can be prevented either by using very low concentrations or by adding surfactants or polymers during the reduction step [121–126]. A number of strategies to combine CRGO materials with polymers can be found in the literature [103, 118, 127–135]. For example, CRGO dispersions were blended together with a polymer latex to produce composites with good electrical properties (∼15 S m^{-1} at ∼1.8 wt.%), and low percolation thresholds (∼0.9 wt.%) [126, 127]. Potts *et al* found similar electrical performances when including CRGO and TRGO into natural rubber (NR) composites, both of which were superior with respect to CB [118, 119].

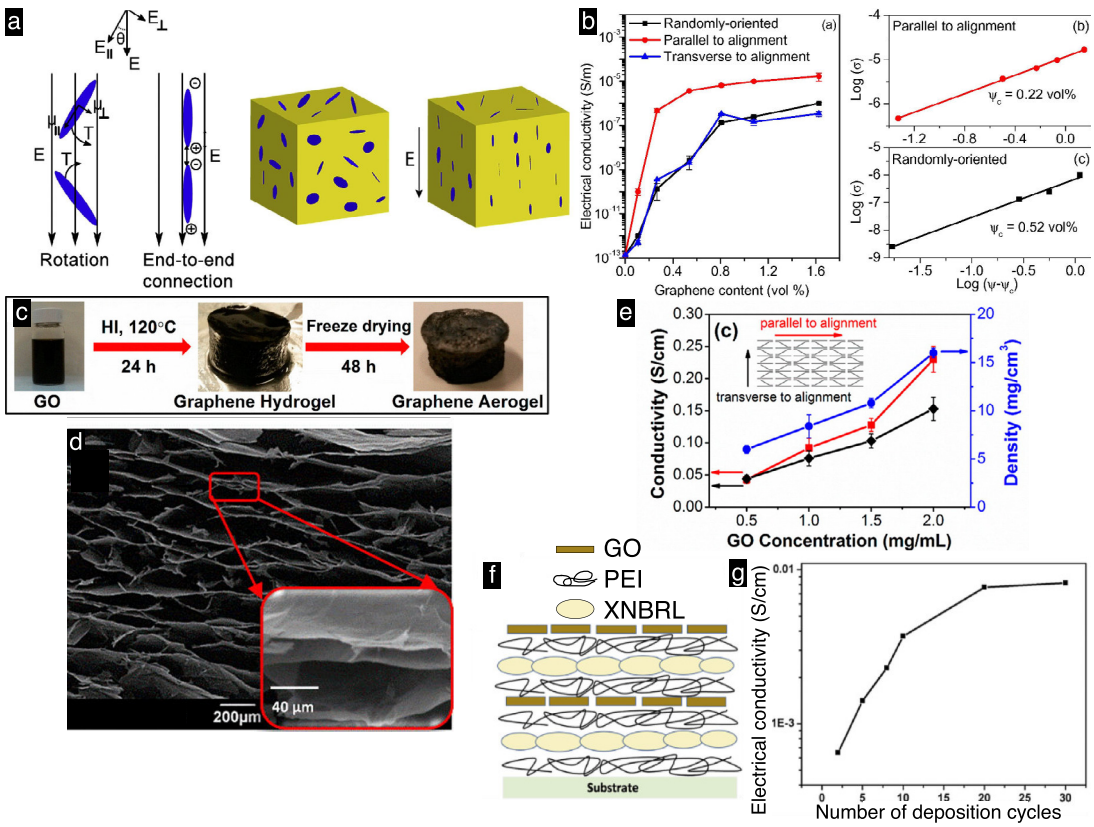

Figure 6. (a) An external electric field can encourage the orientation of a graphene filler, which results in a lower percolation threshold (b) (adapted from [146], CC BY 4.0). (c) Forming a graphene aerogel that displays a laminated structure (d), which can be used as the foundation for an epoxy composite. For this structure, the conductivity is greatest parallel to the alignment of the flakes (e) (adapted from [147], copyright 2015 American Chemical Society). (f) A diagram of a layer-by-layer structure on a substrate; (g) the electrical conductivity of (PEI/XNBR/PEI/GO)n films increases with an increasing number of deposition cycles (adapted from [108], copyright 2015, with permission from Elsevier).

Schopp *et al* performed a comparative study on styrene-butadiene rubber (SBR) composites with the incorporation of different carbon nanofillers [103]. Processed under identical conditions the electrical conductivities of SBR composites for expanded graphite (EG), carbon black (CB) and CRGO were found to be four to five orders of magnitude smaller than those observed for TRGO, MLG and CNTs containing the same amount of carbon filler [103].

4.3.3. *Graphene/CNT hybrid fillers*

One area of increasing interest is the use of a combination of graphene and CNTs as fillers for conducting composites. In many cases the two carbon nanofillers have a synergistic effect, yielding composites that have better performance than those made from the individual components. These hybrid fillers have most successfully been applied in composites that require mechanical strength and electrical conductivity, such as for EMI shielding [136].

The synergistic effect has been seen in a paper formed of graphene and CNTs. The conductivity of the graphene paper was 1.8×10^5 S m^{-1}, but this increased to 2.7×10^5 S m^{-1} with the incorporation of CNTs [137]. For the case of polymer composites, a PU/GNP/CNT composite yielded a conductivity of 10 S m^{-1} after adding graphene and CNTs, which was higher than when adding them individually [136]. The origin of this increase is that the CNTs act as conductivity bridges between the GNP flakes, helping create a conducting network. Another contributing factor is that the CNTs can stop the graphene flakes from re-stacking, encouraging their dispersion in the matrix [138]. Finally, the graphene can also improve the rheological properties of the composite, again encouraging a good dispersion of the fillers [139] and reducing the brittleness of the final composite [140].

4.3.4. *Functionalised graphene*

Functionalised graphene materials are emerging as attractive alternatives to TRGO and CRGO as reinforcements for polymers. The incorporation of functional groups during dry grinding has been recently reported [105]. Nitrogen-containing functional groups can be incorporated by dry grinding in a nitrogen atmosphere, or oxygen groups if a CO_2 atmosphere is used. These functional groups promote interfacial coupling at the filler/epoxy (EP) interfaces, thus improving the dispersion in the host matrix. However, the functional groups did impair the electrical conductivity. As compared to TRGO/EP and N-TRGO/EP composites, the percolation threshold of dry-milled graphene (DMG) has been observed

to increase, due to the significantly lower aspect ratios and lower viscosities of DMG/EP mixtures (as shown in figure 5(d)). Although TRGO materials currently show superior electrical performances, DMGs are still promising because they are cheaper than TRGO and higher filler contents are feasible without impairing processability.

One concept for increasing the electrical conductivity is doping graphene with heteroatoms such as nitrogen [141]. N-doped TRGO produced via thermolysis has been reported to improve the electrical conductivity of both graphene and the corresponding polymer composites [109]. Increases in the nitrogen content from 0 to 12 wt.% were found to increase the electrical conductivity of the graphene material from 4800 to 47 000 S m^{-1} [109]. Nitrogen doping of the graphene filler has been reported to encourage the formation of a continuous conductive path in the host polymer of PA12 [109], polyethylene [142], polypropylene [110], polyurethanes [111], rubber [103], polystyrene [143, 144] and polyamide [112] composites with respect to their TRGO analogues. The electrical percolation thresholds found for the highly exfoliated TRGO and N-TRGO in polymer composites are typically quite low (typically between 1 and 2.5 wt.%) in accordance with their efficient exfoliation and high aspect ratio [105].

4.4. Nanostructured architectures

The alignment of the conductive fillers also plays a role in the conductivity in composites [145]. Kim *et al* [93] prepared three sets of polycarbonate samples reinforced with few-layer graphene initially by melt blending and then moulded into three different geometries. They found that compression moulding encouraged the alignment of the platelet-shaped particles, but did prevent connectivity between them, and so ultimately reduced the conductivity. In another example, Wu *et al* [146] prepared epoxy/GNP composites where they induced an alignment of the flakes by applying an external electric field as shown in figure 6(a). The conductivities of the composites in the direction of alignment were 2–3 orders of magnitude higher than that along the transverse direction as seen in figure 6(b).

To encourage efficient contact between fillers, one possible strategy is to assemble the graphene sheets into layered structures [148]. For example, Yousefiu *et al* [128, 149, 150] have recently reported the synthesis of self-aligned, layered, CRGO/epoxy composites by simultaneous *in situ* reduction and self-alignment of GO sheets. Furthermore, the *in situ* polymerization procedure used enabled the formation of strong chemical bonds between the filler and the host epoxy matrix. The resulting materials displayed significantly improved electrical properties in the alignment direction, yielding a percolation threshold of 0.12 vol.%. A further increase in CRGO content beyond 2 wt.% resulted in an ultimate conductivity above 1 S m^{-1}, which is high enough for many practical applications, such as antistatic coatings, electromagnetic interference (EMI) shields and thermal conductors.

The electrical conductivities of graphene/polymer nanocomposites prepared by direct dispersion of GNPs or CRGO sheets into the polymer (including those containing highly aligned and well-dispersed ultra-large graphene sheets) are, however, commonly still below 10 S m^{-1} [150]. The formation of a 3D interconnected conductive network within the insulating polymer matrix has recently emerged as a more efficient way to improve the electrical conductivity [151–153]. As an example, Wang *et al* [147] recently reported the synthesis of graphene aerogels (GAs) through one-step chemical reduction and rational self-assembly of GO sheets using hydroiodic (HI) acid, followed by freeze-drying and vacuum-assisted epoxy infiltration (as shown in figure 6(c)). The porous microstructure of the resulting GA is clearly seen in the SEM image shown in figure 6(d). This preparation method produced a composite with remarkable electrical conductivities of 4–25 S m^{-1} depending on the concentration of CRGO, as seen in figure 6(e). The percolation threshold for the GA/epoxy composites was found to be ~0.25 wt.%, with the highest conductivity of 20 S m^{-1} obtained at 1.4 wt.% graphene content, which is 4 orders of magnitude higher than that found for 2.0 wt.% GNP [154], and nearly 2 orders of magnitude higher than those containing 3 wt.% CRGO [128] or 1 wt.% CNTs [155].

The formation of hydrogels from graphene/polymer composites has also begun to attract attention [156]. Here, the inclusion of GO into the polymer increases the polymer's ability to uptake water. This water uptake can be tuned, which in turn can lead to a tunable electrical conductivity. She *et al* investigated the conductivity of a PPy/GO composite after repeated cycling treatments of soaking in HCl and NaOH [157]. After HCl soaking the conductivity increased to ~0.1 S m^{-1}, and after NaOH soaking it decreased to ~1×10^{-4} S m^{-1}. These graphene composites could be used in chemical sensing applications.

4.5. Layer-by-layer (LbL) assembly

Layer-by-layer (LbL) assembly has been widely used to fabricate graphene-containing, ultrathin films or graphene-based polymer composite films [158–160]. These highly ordered assemblies offer nanometre precision of filler placement and so could help create ideal nanocomposite structures. The LbL self-assembly strategy has recently been used for the development of graphene-based elastomer nanocomposites. For example, highly ordered free-standing multilayer films of alternating negatively charged GO sheets, positively charged polyethyleneimine (PEI), and negatively charged carboxylic acrylonitrile butadiene rubber (XNBR) latex have been successfully fabricated by electrostatic LbL self-assembly [108]. The structure of this LbL composite is shown in figure 6(f). The

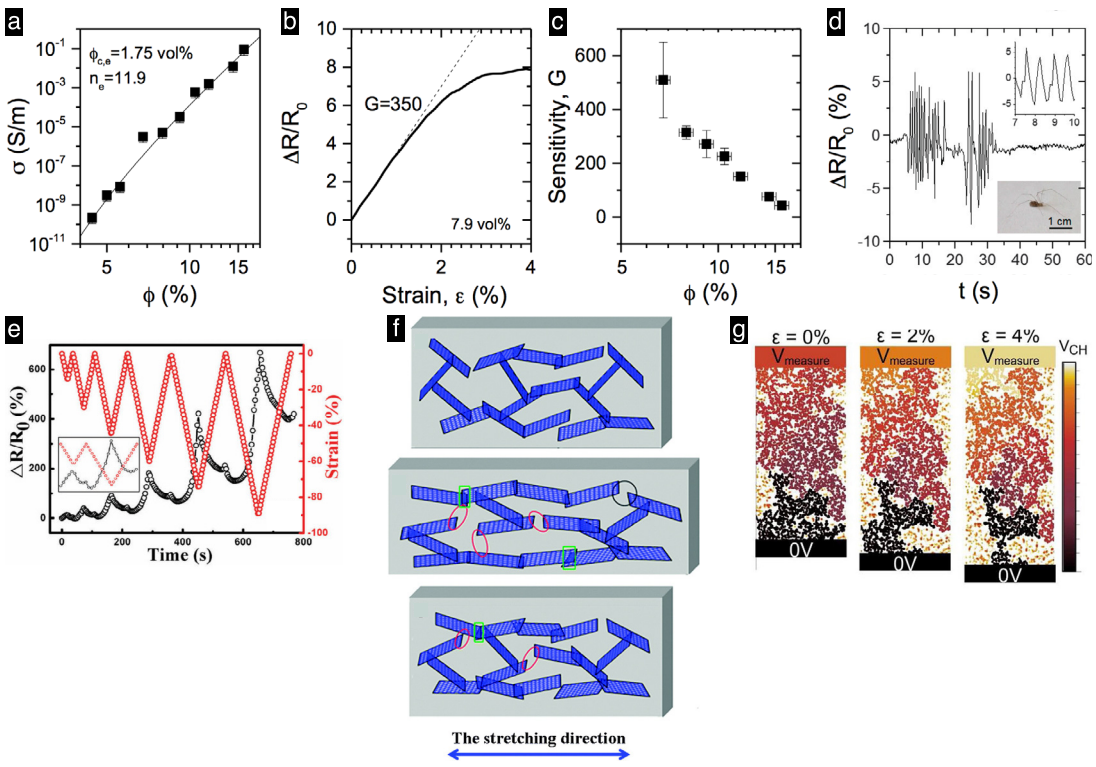

Figure 7. (a) Conductivity as a function of volume fraction for polysilicone/graphene composites with the solid line representing percolation theory. (b) Resistance change as a function of strain for a 7.9 vol% composite. (c) the sensor sensitivity (gauge factor) as a function of graphene volume fraction. (d) The polysilicone/graphene composite employed as an impact sensor, monitoring the footsteps of a small spider (adapted from [163] with permission from AAAS). (e) A graphene/TPU composite sensor performs repeatedly over successive cycles (adapted from [164] with permission of The Royal Society of Chemistry). (f) The effect of strain on a percolating composite; filler connection are broken (and sometimes reformed), changing the composites conductivity (adapted from [165] with permission of The Royal Society of Chemistry). (g) Modelling the voltage drop across a composite's filler network as it is strained (adapted from [162], copyright 2012 American Chemical Society).

conductivity of these multilayer films was found to increase with increasing number of GO layers (from 6.5×10^{-2} S m^{-1} to 0.82 S m^{-1} as their deposition cycles increased from 2 to 30), as shown in figure 6(g).

The fabrication of electrically conductive graphene/PS composite films by combining latex technology with LbL assembly has also been recently reported [129]. In this work, percolation in graphene/PS composites was observed with the assembly of only one layer of graphene when the filler concentration was around 0.2 vol.%. The electrical conductivities were found to increase dramatically from 7×10^{-7} S m^{-1} to 0.02 S m^{-1} as the number of bilayers was increased from one to two (i.e. 0.9 vol.%), and to a value of 0.05 S m^{-1} with three bilayers (1.3 vol.%).

5. Effect of strain on percolated networks

A major application that exploits the electrical percolation behaviour of graphene nanocomposites is resistive strain sensors. Here strain on the composite causes a change in its microstructure and so causes a change in its electrical resistance [161]. A key metric of resistive strain sensors is the strength of this effect, called the gauge factor, and is defined as:

$$GF = \frac{R/R_0}{\epsilon} \qquad (6)$$

where R_0 is the unstrained resistance, and R is the resistance at an applied strain ϵ (for low strains).

Graphene was first applied as a thin film of graphene platelets spray cast onto a flexible plastic substrate [162]. The platelets overlapped in regions and they formed a conductive network, whose resistance changed under strain. They found that the *GF* could be tuned by controlling the degree of overlap, which was done by controlling the concentrations of the deposition. A maximum *GF* of 150 was recorded. An advantage of this method is that the flakes can be directly deposited onto any substrate, but the system was limited to only small strains.

Better performance over greater strains is possible by embedding graphene in a flexible nanocomposite. For example, graphene in a rubber matrix produced a $GF = 35$ that could operate up to strains of 800% [5]. More recently, combining graphene in a similar way with highly viscoelastic silicone polymer (commonly known as Silly Putty^{TM}) yielded a composite material with variable conductivity as described by classic percolation theory [163]. Figure 7(a) shows that the composite had a percolation threshold of 1.75 vol%, and (b) shows that a composite with 7.9 vol% loading had a gauge factor of 350 at low strain. At loadings closer to the percolation threshold the sensors were even more sensitive, with values up to 500 measured as shown in figure 7(c). This sensitivity allowed them to monitor

breathing and pulse, as well as the movement of a spider (as shown in figure 7(d)).

Graphene sensors can also be formed from porous graphene structures that can then be filled with polymer. Using this method gauge factors up to 11 were achieved with a GNP-PDMS sensor [166]. The GNP network was formed by pressing the flakes onto a substrate and then allowing PDMS to diffuse into the network.

Structured graphene nanocomposites can also be formed after the matrix and filler have been mixed. A graphene-TPU mixture was freeze dried to give a structure with 90% porosity and a low density of 0.11 g cm^{-3} [164]. While these structures produced only low gauge factors (~2) they performed well under successive compressive testing (figure 7(e)).

The mechanism of resistance change is a combination of two processes, both of which depend upon the microstructure of the conducting network. The first is that as the composite stretches the number of conductive pathways is reduced as graphene flakes become separated [165] (figure 7(f)). The second mechanism involves disconnected but closely spaced graphene sheets that the charge carriers can tunnel between; as these sheets become more separated, the tunnelling current diminishes [165]. This can also be seen by modelling the voltage drop that occurs through the network as it is strained: figure 7(g) shows how the voltage drop is more pronounced as the material is strained because fewer conductive paths are available [162]. The process of breaking and forming junctions is often reversible and hence the graphene–polymer composites are able to perform many strain cycles (e.g. 400 cycles with 60% strain [167]) before failure.

6. Conclusions

In conclusion, graphene of various types has successfully been used as a filler to create conductive composites from insulating polymers. Of all the carbon nanofillers, GRMs remain the most promising candidates for electrically conductive polymer composites because of their large surface areas, large aspect ratios, and high electrical conductivities. They have yielded composites with very low percolation thresholds, and in addition, have shown to be easier to prepare at higher loadings, giving better ultimate conductivities.

In choosing a graphene filler, there is a careful balance between production and performance. The highest conducting graphene (that which has been mechanically exfoliated) cannot be produced in quantities needed for polymer fillers. However, solution-based techniques, which can produce the volumes required, tend to produce material with lower conductivity. However, recent years has seen this improve. There are now liquid exfoliation methods available that do not require covalent functionalisation of the graphene, and so produce material with very high intrinsic conductivities, albeit with some reduction in aspect ratio. At the same time, there has been consistent improvement in the ability to reduce GO to return its conductivity. This has perhaps yielded the most success in conductive composites, as the few remaining functional groups after reduction do play an important role in encouraging better dispersion in the matrix. Graphene production methods should prioritise producing larger, thinner sheets, that remain defect-free. Greater control of the functionalisation of the graphene sheets should also be explored. Careful tailoring of functional groups could yield an ideal conductive filler that disperses well while still maintaining a high conductivity.

Finally, applications for electrically percolating graphene composites have started to appear. Strain sensors show promise, with high sensitivities displayed from composites that are easy to produce. There is still a need to create networks that are more reproducible, and stable for longer. The promise here lies in greater nanoscale control from deliberate structuring of the composites.

Appendix. Abbreviations

ABS, Acrylonitrile butadiene styrene; BA, Butyl acrylate; CB, Carbon black; CNT, Carbon nanotube; CRGO, Chemically reduced graphene oxide; CVD, Chemical vapour deposition; DMG, Dry-milled graphene; DOS, Density of states; EG, Expanded graphite; EMI, Electromagnetic interference; EP, Epoxy; f-GNP, Functionalised-graphite nanoplatelets; GA, Graphene aerogels; GNP, Graphite nanoplatelets; GNS, Graphene nanosheets; GO, Graphene oxide; GRM, Graphene related materials; HDPE, High-density polyethylene; HI, Hydroiodic acid; iPP, Isotactic polypropylene; LbL, Layer-by-layer; LLDPE, Linear low-density polyethylene; MLG, Multilayer graphene; N-TRGO, Nitrogen-thermally reduced graphene oxide; NR, Natural rubber; PA11, Polyamide 11; PA12, Polyamide 12; PA6, Polyamide 6; PC, Polycarbonate; PCL, Polycaprolactone; PE, Polyethylene; PEI, Polyethyleneimine; PI, Polyimide; PLA, Polylactic acid; PMMA, Poly(methyl methacrylate); POSS, Polyhedral oligomeric silsesquioxane; PP, Polypropylene; PS, Polystyrene; PU, Polyurethane; PVC, Polyvinyl chloride; rGO, Reduced-graphene oxide; SAN, Styrene-acrylonitrile; SBR, Styrene-butadiene; sPS, Syndiotactic polystyrene; TPU, Thermoplastic polyurethane; TRGO, Thermally reduced graphene oxide; UHMWPE, Ultra-high-molecular-weight polyethylene; VRH, Variable range hopping; XNBR, Carboxylated nitrile butadiene rubber.

ORCID iDs

A J Marsden https://orcid.org/0000-0002-3017-1754
D G Papageorgiou https://orcid.org/0000-0001-5558-5040

C Vallés https://orcid.org/0000-0002-9359-1705
A Liscio https://orcid.org/0000-0003-2986-3398
V Palermo https://orcid.org/0000-0002-0168-9693
M A Bissett https://orcid.org/0000-0002-8908-7960
R J Young https://orcid.org/0000-0001-6073-9489
I A Kinloch https://orcid.org/0000-0003-3314-6869

References

[1] Kim J, Yim B S, Kim J M and Kim J 2012 *Microelectron. Reliab.* **52** 595–602
[2] Raimondo M, Guadagno L, Speranza V, Bonnaud L, Dubois P and Lafdi K 2018 *Compos. Part B: Eng.* **140** 44–56
[3] Jan R, Habib A, Akram M A, Ahmad I, Shah A, Sadiq M and Hussain A 2017 *Mater. Res. Express* **4** 035605
[4] Wang H, Xie G, Fang M, Ying Z, Tong Y and Zeng Y 2015 *Compos. Part B: Eng.* **79** 444–50
[5] Boland C S *et al* 2014 *ACS Nano* **8** 8819–30
[6] Bauhofer W and Kovacs J Z 2009 *Compos. Sci. Technol.* **69** 1486–98
[7] Balberg I 2002 *Carbon* **40** 139–43
[8] Gojny F H, Wichmann M H G, Fiedler B, Kinloch I A, Bauhofer W, Windle A H and Schulte K 2006 *Polymer* **47** 2036–45
[9] Li F, Qi L, Yang J, Xu M, Luo X and Ma D 2000 *J. Appl. Polym. Sci.* **75** 68–77
[10] Lee S H, Kim M W, Kim S H and Youn J R 2008 *Eur. Polym. J.* **44** 1620–30
[11] Socher R, Krause B, Müller M T, Boldt R and Pötschke P 2012 *Polymer* **53** 495–504
[12] Suarez-Martinez I, Grobert N and Ewels C P 2012 *Carbon* **50** 741–7
[13] Ferrari A C *et al* 2015 *Nanoscale* **7** 4598–810
[14] Du X, Skachko I, Barker A and Andrei E Y 2008 *Nat. Nanotechnol.* **3** 491–5
[15] Kuilla T, Bhadra S, Yao D H, Kim N H, Bose S and Lee J H 2010 *Prog. Polym. Sci.* **35** 1350–75
[16] Sengupta R, Bhattacharya M, Bandyopadhyay S and Bhowmick A K 2011 *Prog. Polym. Sci.* **36** 638–70
[17] Li X, Zhu Y, Cai W, Borysiak M, Han B, Chen D, Piner R D, Colombo L and Ruoff R S 2009 *Nano Lett.* **9** 4359–63
[18] Reina A, Jia X, Ho J, Nezich D, Son H, Bulovic V, Dresselhaus M S and Kong J 2009 *Nano Lett.* **9** 30–5
[19] Banhart F, Kotakoski J and Krasheninnikov A V 2011 *ACS Nano* **5** 26–41
[20] Hao Y *et al* 2013 *Science* **342** 720–3
[21] Lee G D, Yoon E, He K, Robertson A W and Warner J H 2014 *Nanoscale* **6** 14836–44
[22] Buron J D *et al* 2014 *Nano Lett.* **14** 6348–55
[23] Chen Y, Gong X L and Gai J G 2016 *Adv. Sci.* **3** 1–15
[24] Hummers W S, Offeman R E, Hummers W S Jr, Offeman R E, Hummers W S and Offeman R E 1958 *J. Am. Chem. Soc.* **80** 1339
[25] Brodie B C 1859 *Phil. Trans. R. Soc. Lond.* **149** 249–59
[26] Staudenmaier L 1898 *Ber. Dtsch. Chem. Ges* **31**
[27] Marcano D C, Kosynkin D V, Berlin J M, Sinitskii A, Sun Z, Slesarev A, Alemany L B, Lu W and Tour J M 2010 *ACS Nano* **4** 4806–14
[28] Mohan V B, Brown R, Jayaraman K and Bhattacharyya D 2015 *Mater. Sci. Eng.* B **193** 49–60
[29] Stankovich S, Dikin D A, Piner R D, Kohlhaas K A, Kleinhammes A, Jia Y, Wu Y, Nguyen S T B T and Ruoff R S 2007 *Carbon* **45** 1558–65
[30] Mattevi C, Eda G, Agnoli S, Miller S, Mkhoyan K A, Celik O, Mastrogiovanni D, Granozzi G, Carfunkel E and Chhowalla M 2009 *Adv. Funct. Mater.* **19** 2577–83
[31] Mohan V B, Jakisch L, Jayaraman K and Bhattacharyya D 2018 *Mater. Res. Express* **5** 035604
[32] Shin H J *et al* 2009 *Adv. Funct. Mater.* **19** 1987–92
[33] Finn D J, Lotya M, Cunningham G, Smith R J, McCloskey D, Donegan J F and Coleman J N 2014 *J. Mater. Chem.* C **2** 925–32
[34] Dreyer D R, Park S, Bielawski C W and Ruoff R S 2010 *Chem. Soc. Rev.* **39** 228–40
[35] Chen W, Yan L and Bangal P R 2010 *J. Phys. Chem.* C **114** 19885–90
[36] Gómez-Navarro C *et al* 2007 *Nano Lett.* **7** 3499–503
[37] Liu C, Hao F, Zhao X, Zhao Q, Luo S and Lin H 2015 *Sci. Rep.* **4** 3965
[38] Mativetsky J M, Treossi E, Orgiu E, Melucci M, Veronese G P, Samorì P and Palermo V 2010 *J. Am. Chem. Soc.* **132** 14130–6
[39] Mativetsky J M, Liscio A, Treossi E, Orgiu E, Zanelli A, Samorì P and Palermo V 2011 *J. Am. Chem. Soc.* **133** 14320–6
[40] Vianelli A, Candini A, Treossi E, Palermo V and Affronte M 2015 *Carbon* **89** 188–96
[41] Becerril H A, Mao J, Liu Z, Stoltenberg R M, Bao Z and Chen Y 2008 *ACS Nano* **2** 463–70
[42] Yang H, Cao Y, He J, Zhang Y, Jin B, Sun J L, Wang Y and Zhao Z 2017 *Carbon* **115** 561–70
[43] Wu Z S, Ren W, Gao L, Zhao J, Chen Z, Liu B, Tang D, Yu B, Jiang C and Cheng H M 2009 *ACS Nano* **3** 411–7
[44] De S, King P J, Lotya M, O'Neill A, Doherty E M, Hernandez Y, Duesberg G S and Coleman J N 2010 *Small* **6** 458–64
[45] Paton K R *et al* 2014 *Nat. Mater.* **13** 624–30
[46] Hernandez Y *et al* 2008 *Nat. Nanotechnol.* **3** 563–8
[47] Lotya M *et al* 2009 *J. Am. Chem. Soc.* **131** 3611–20
[48] Meng Q, Jin J, Wang R, Kuan H C, Ma J, Kawashima N, Michelmore A, Zhu S and Wang C H 2014 *Nanotechnology* **25** 125707–19
[49] Nan C W, Shen Y and Ma J 2010 *Ann. Rev. Mater. Res.* **40** 131–51
[50] Balberg I, Azulay D, Toker D and Millo O 2004 *Int. J. Mod. Phys.* B **18** 2091–121
[51] Jović N, Dudić D, Montone A, Antisari M V, Mitrić M and Djoković V 2008 *Scr. Mater.* **58** 846–9
[52] Ambrosetti G, Grimaldi C, Balberg I, Maeder T, Danani A and Ryser P 2010 *Phys. Rev.* B **81** 155434
[53] Trionfi A, Scrymgeour D A, Hsu J W P, Arlen M J, Tomlin D, Jacobs J D, Wang D H, Tan L S and Vaia R A 2008 *J. Appl. Phys.* **104** 83708
[54] Kim H, Kobayashi S, AbdurRahim M A, Zhang M J, Khusainova A, Hillmyer M A, Abdala A A and Macosko C W 2011 *Polymer* **52** 1837–46
[55] Pötschke P, Bhattacharyya A R and Janke A 2003 *Polymer* **44** 8061–9
[56] Zhang H B, Zheng W G, Yan Q, Yang Y, Wang J W, Lu Z H, Ji G Y and Yu Z Z 2010 *Polymer* **51** 1191–6
[57] Du J, Zhao L, Zeng Y, Zhang L, Li F, Liu P and Liu C 2011 *Carbon* **49** 1094–100
[58] Ambrosetti G, Johner N, Grimaldi C, Danani A and Ryser P 2008 *Phys. Rev.* E **78** 61126
[59] Li J and Kim J K 2007 *Compos. Sci. Technol.* **67** 2114–20
[60] Fournier J, Boiteux G, Seytre G and Marichy G 1997 *Synth. Met.* **84** 839–40
[61] Essam J W 1980 *Rep. Prog. Phys.* **43** 833
[62] Gao J F, Li Z M, Meng Q J and Yang Q 2008 *Mater. Lett.* **62** 3530–2
[63] Stauffer D and Aharony A 1994 *Introduction to Percolation Theory* (Boca Raton, FL: CRC Press)
[64] Simmons J G 1963 *J. Appl. Phys.* **34** 1793–803
[65] Hicks J, Behnam A and Ural A 2009 *Appl. Phys. Lett.* **95**
[66] Yu Y, Song G and Sun L 2010 *J. Appl. Phys.* **108**
[67] Zabihi Z and Araghi H 2016 *Synth. Met.* **217** 87–93
[68] Bao W S, Meguid S A, Zhu Z H, Pan Y and Weng G J 2012 *Mech. Mater.* **46** 129–38
[69] Hashemi R and Weng G J 2016 *Carbon* **96** 474–90
[70] Xia X, Wang Y, Zhong Z and Weng G J 2017 *Carbon* **111** 221–30
[71] Zhao S, Lou D, Zhan P, Li G, Dai K, Guo J, Zheng G, Liu C, Shen C and Guo Z 2017 *J. Mater. Chem.* C **5** 8233–42
[72] Cattani M, Salvadori M C and Cattani M 2009 1–11 arXiv:0903.3587
[73] van Hapert J J 2002 *PhD Thesis* (Utrecht University)
[74] Kaiser A B, Subramaniam C K, Gilberd P W and Wessling B 1995 *Synth. Met.* **69** 197–200
[75] Mott N F 1969 *Contemp. Phys.* **10** 125–38
[76] Joung D and Khondaker S I 2012 *Phys. Rev.* B **86**

[77] Vlassiouk I, Polizos G, Cooper R, Ivanov I, Keum J K, Paulauskas F, Datskos P and Smirnov S 2015 *ACS Appl. Mater. Interfaces* **7** 10702–9
[78] Liu P *et al* 2016 *Science* **353** 364–7
[79] Qi X Y, Yan D, Jiang Z, Cao Y K, Yu Z Z, Yavari F and Koratkar N 2011 *ACS Appl. Mater. Interfaces* **3** 3130–3
[80] Wu H, Rook B and Drzal L T 2013 *Polymer Compos.* **34** 426–32
[81] Pang H, Chen T, Zhang G, Zeng B and Li Z M 2010 *Mater. Lett.* **64** 2226–9
[82] Kim H, Miura Y and Macosko C W 2010 *Chem. Mater.* **22** 3441–50
[83] Xu H, Gong L X, Wang X, Zhao L, Pei Y B, Wang G, Liu Y J, Wu L B, Jiang J X and Tang L C 2016 *Compos. Part A: Appl. Sci. Manuf.* **91, Part 1** 53–64
[84] Vallés C, Abdelkader A M, Young R J and Kinloch I A 2014 *Faraday Discuss.* **173** 379–90
[85] Vallés C, Abdelkader A M, Young R J and Kinloch I A 2015 *Compos. Sci. Technol.* **111** 17–22
[86] Papageorgiou D G, Kinloch I A and Young R J 2016 *Compos. Sci. Technol.* **137** 44–51
[87] You F, Li X, Zhang L, Wang D, Shi C Y and Dang Z M 2017 *RSC Adv.* **7** 6170–8
[88] Yan D, Zhang H B, Jia Y, Hu J, Qi X Y, Zhang Z and Yu Z Z 2012 *ACS Appl. Mater. Interfaces* **4** 4740–5
[89] Gao Y, Picot O T, Tu W, Bilotti E and Peijs T 2018 *J. Appl. Polym. Sci.* **135** 46041
[90] Li X, McKenna G B, Miquelard-Garnier G, Guinault A, Sollogoub C, Regnier G and Rozanski A 2014 *Polymer* **55** 248–57
[91] Carotenuto G, De Nicola S, Palomba M, Pullini D, Horsewell A, Hansen T W and Nicolais L 2012 *Nanotechnology* **23** 485705
[92] Gaska K, Xu X, Gubanski S and Kádár R 2017 *Polymers* **9** 11
[93] Kim H and Macosko C W 2009 *Polymer* **50** 3797–809
[94] Wu H and Drzal L T 2013 *J. Appl. Polym. Sci.* **130** 4081–9
[95] Wu H and Drzal L T 2016 *Mater. Chem. Phys.* **182** 110–8
[96] Arzac A, Leal G P, Fajgar R and Tomovska R 2014 *Part. Part. Syst. Charact.* **31** 143–51
[97] Arzac A, Leal G P, de la Cal J C and Tomovska R 2017 *Macromol. Mater. Eng.* **302** 1600315
[98] Dikin D A, Stankovich S, Zimney E J, Piner R D, Dommett G H B, Evmenenko G, Nguyen S T and Ruoff R S 2007 *Nature* **448** 457–60
[99] Vickery J L, Patil A J and Mann S 2009 *Adv. Mater.* **21** 2180–4
[100] McAllister M J *et al* 2007 *Chem. Mater.* **19** 4396–404
[101] Bourlinos A B, Gournis D, Petridis D, Szabo T, Szeri A and Dekany I 2003 *Langmuir* **19** 6050–5
[102] Steurer P, Wissert R, Thomann R and Mülhaupt R 2009 *Macromol. Rapid Commun.* **30** 316–27
[103] Schopp S, Thomann R, Ratzsch K F, Kerling S, Altstadt V, Mulhaupt R, Altstädt V, Mülhaupt R, Altstadt V and Mulhaupt R 2014 *Macromol. Mater. Eng.* **299** 319–29
[104] Vasileiou A A, Kontopoulou M and Docoslis A 2014 *ACS Appl. Mater. Interfaces* **6** 1916–25
[105] Tschoppe K, Beckert F, Beckert M and Mülhaupt R 2015 *Macromol. Mater. Eng.* **300** 140–52
[106] Zhang H B, Zheng W G, Yan Q, Jiang Z G and Yu Z Z 2012 *Carbon* **50** 5117–25
[107] Aguilar-Bolados H, Brasero J, Lopez-Manchado M A and Yazdani-Pedram M 2014 *Compos. Part B: Eng.* **67** 449–54
[108] Wang L, Wang W, Fu Y, Wang J, Lvov Y, Liu J, Lu Y and Zhang L 2016 *Compos. Part B: Eng.* **90** 457–64
[109] Beckert M, Tölle F J, Bruchmann B and Mülhaupt R 2015 *Macromol. Mater. Eng.* **300** 785–92
[110] Hofmann D, Wartig K A, Thomann R, Dittrich B, Schartel B and Mulhaupt R 2013 *Macromol. Mater. Eng.* **298** 1322–34
[111] Appel A K, Thomann R and Mulhaupt R 2012 *Polymer* **53** 4931–9
[112] Hofmann D, Keinath M, Thomann R and Mülhaupt R 2014 *Macromol. Mater. Eng.* **299** 1329–42
[113] Zheng W, Lu X H and Wong S C 2004 *J. Appl. Polym. Sci.* **91** 2781–8
[114] Cerezo F T, Preston C M L and Shanks R A 2007 *Macromol. Mater. Eng.* **292** 155–68
[115] Chen G H, Weng W G, Wu D J and Wu C L 2003 *Eur. Polym. J.* **39** 2329–35
[116] Cerezo F T, Preston C M L and Shanks R A 2007 *Compos. Sci. Technol.* **67** 79–91
[117] Kim J S, Hong S, Park D W and Shim S E 2010 *Macromol. Res.* **18** 558–65
[118] Potts J R, Shankar O, Du L and Ruoff R S 2012 *Macromolecules* **45** 6045–55
[119] Potts J R, Shankar O, Murali S, Du L and Ruoff R S 2013 *Compos. Sci. Technol.* **74** 166–72
[120] Kim J S, Yun J H, Kim I and Shim S E 2011 *J. Ind. Eng. Chem.* **17** 325–30
[121] Li D, Müller M B, Gilje S, Kaner R B and Wallace G G 2008 *Nat. Nanotechnol.* **3** 101–5
[122] Fang M, Wang K, Lu H, Yang Y and Nutt S 2010 *J. Mater. Chem.* **20** 1982–92
[123] Liang Y, Wu D, Feng X and Müllen K 2009 *Adv. Mater.* **21** 1679–83
[124] Lee D Y, Yoon S, Oh Y J, Park S Y and In I 2011 *Macromol. Chem. Phys.* **212** 336–41
[125] Stankovich S, Piner R D, Chen X, Wu N, Nguyen S T and Ruoff R S 2006 *J. Mater. Chem.* **16** 155–8
[126] Wissert R, Steurer P, Schopp S, Thomann R and Mulhaupt R 2010 *Macromol. Mater. Eng.* **295** 1107–15
[127] Tkalya E, Ghislandi M, Alekseev A, Koning C and Loos J 2010 *J. Mater. Chem.* **20** 3035–9
[128] Yousefi N, Lin X, Zheng Q, Shen X, Pothnis J R, Jia J, Zussman E and Kim J K 2013 *Carbon* **59** 406–17
[129] Fan W, Zhang C, Tjiu W W and Liu T X 2013 *J. Mater. Res.* **28** 611–9
[130] Ha H W, Choudhury A, Kamal T, Kim D H and Park S Y 2012 *ACS Appl. Mater. Interfaces* **4** 4623–30
[131] Wang X, Hu Y, Song L, Yang H, Xing W and Lu H 2011 *J. Mater. Chem.* **21** 4222
[132] Zhan Y, Lavorgna M, Buonocore G and Xia H 2012 *J. Mater. Chem.* **22** 10464–8
[133] Huang Y J, Qin Y W, Wang N, Zhou Y, Niu H, Dong J Y, Hu J P and Wang Y X 2012 *Macromol. Chem. Phys.* **213** 720–8
[134] Hu H T, Wang X B, Wang J C, Wan L, Liu F M, Zheng H, Chen R and Xu C H 2010 *Chem. Phys. Lett.* **484** 247–53
[135] Shen Y X, Jing T, Ren W J, Zhang J W, Jiang Z G, Yu Z Z and Dasari A 2012 *Compos. Sci. Technol.* **72** 1430–5
[136] Verma M, Chauhan S S, Dhawan S K and Choudhary V 2017 *Compos. Part B: Eng.* **120** 118–27
[137] Zhou E, Xi J, Guo Y, Liu Y, Xu Z, Peng L, Gao W, Ying J, Chen Z and Gao C 2018 *Carbon* https://doi.org/10.1016/j.carbon.2018.03.023
[138] Oh J Y, Jun G H, Jin S, Ryu H J and Hong S H 2016 *ACS Appl. Mater. Interfaces* **8** 3319–25
[139] Kuester S, Demarquette N R, Ferreira J C, Soares B G and Barra G M 2017 *Eur. Polym. J.* **88** 328–39
[140] Kugler S, Kowalczyk K and Spychaj T 2015 *Prog. Org. Coat.* **85**
[141] Khai T V, Na H G, Kwak D S, Kwon Y J, Ham H, Shim K B and Kim H W 2012 *J. Mater. Chem.* **22** 17992–8003
[142] Sturzel M, Thomann Y, Enders M and Mulhaupt R 2014 *Macromolecules* **47** 4979–86
[143] Beckert F, Friedrich C, Thomann R and Mulhaupt R 2012 *Macromolecules* **45** 7083–90
[144] Beckert F, Rostas A M, Thomann R, Weber S, Schleicher E, Friedrich C and Mulhaupt R 2013 *Macromolecules* **46** 5488–96
[145] Du F, Fischer J E and Winey K I 2005 *Phys. Rev.* B **72** 121404
[146] Wu S, Ladani R B, Zhang J, Bafekrpour E, Ghorbani K, Mouritz A P, Kinloch A J and Wang C H 2015 *Carbon* **94** 607–18
[147] Wang Z, Shen X, Akbari Garakani M, Lin X, Wu Y, Liu X, Sun X and Kim J K 2015 *ACS Appl. Mater. Interfaces* **7** 5538–49
[148] Ansari S, Kelarakis A, Estevez L and Giannelis E P 2010 *Small* **6** 205–9
[149] Yousefi N, Gudarzi M M, Zheng Q, Aboutalebi S H, Sharif F and Kim J K 2012 *J. Mater. Chem.* **22** 12709–17
[150] Yousefi N, Sun X, Lin X, Shen X, Jia J, Zhang B, Tang B, Chan M and Kim J K 2014 *Adv. Mater.* **26** 5480–7
[151] Jia J, Sun X, Lin X, Shen X, Mai Y W and Kim J K 2014 *ACS Nano* **8** 5774–83

[152] Qiu L, Liu D, Wang Y, Cheng C, Zhou K, Ding J, Truong V T and Li D 2014 *Adv. Mater.* **26** 3333–7
[153] Tang G Q, Jiang Z G, Li X F, Zhang H B, Dasari A and Yu Z Z 2014 *Carbon* **77** 592–9
[154] Chandrasekaran S, Seidel C and Schulte K 2013 *Eur. Polym. J.* **49** 3878–88
[155] Li J, Ma P C, Chow W S, To C K, Tang B Z and Kim J K 2007 *Adv. Funct. Mater.* **17** 3207–15
[156] Ji J, Yu X, Cheng P, Zhang Q, Du F, Li L and Shang S 2015 *J. Macromol. Sci. Part B: Phys.* **54** 1122–31
[157] She X, Sun P, Yu X, Zhang Q, Wu Y, Li L, Huang Y, Shang S and Jiang S 2014 *J. Inorg. Organometallic Polym. Mater.* **24** 884–9
[158] Kulkarni D D, Choi I, Singamaneni S S and Tsukruk V V 2010 *ACS Nano* **4** 4667–76
[159] Wang D G and Wang X G 2011 *Langmuir* **27** 2007–13
[160] Zhao X, Zhang Q H, Hao Y P, Li Y Z, Fang Y and Chen D J 2010 *Macromolecules* **43** 9411–6
[161] Amjadi M, Kyung K U, Park I and Sitti M 2016 *Adv. Funct. Mater.* **26** 1678–98
[162] Hempel M, Nezich D, Kong J and Hofmann M 2012 *Nano Lett.* **12** 5714–8
[163] Boland C S *et al* 2016 *Science* **354** 1257–60
[164] Liu H, Dong M, Huang W, Gao J, Dai K, Guo J, Zheng G, Liu C, Shen C and Guo Z 2017 *J. Mater. Chem.* C **5** 73–83
[165] Liu H, Li Y, Dai K, Zheng G, Liu C, Shen C, Yan X, Guo J and Guo Z 2016 *J. Mater. Chem.* C **4** 157–66
[166] Shi G, Zhao Z, Pai J H, Lee I, Zhang L, Stevenson C, Ishara K, Zhang R, Zhu H and Ma J 2016 *Adv. Funct. Mater.* **26** 7614–25
[167] Lin Y, Dong X, Liu S, Chen S, Wei Y and Liu L 2016 *ACS Appl. Mater. Interfaces* **8** 24143–51
[168] Gao C, Zhang S, Wang F, Wen B, Han C, Ding Y and Yang M 2014 *ACS Appl. Mater. Interfaces* **6** 12252–60
[169] Zheng D, Tang G, Zhang H B, Yu Z Z, Yavari F, Koratkar N, Lim S H and Lee M W 2012 *Compos. Sci. Technol.* **72** 284–9
[170] Rashmi B J, Prashantha K, Lacrampe M F and Krawczak P 2016 *Adv. Polym. Technol.* https://doi.org/10.1002/adv.21757
[171] Xu C, Gao J, Xiu H, Li X, Zhang J, Luo F, Zhang Q, Chen F and Fu Q 2013 *Compos. Part A: Appl. Sci. Manuf.* **53** 24–33
[172] Yoonessi M and Gaier J R 2010 *ACS Nano* **4** 7211–20
[173] Nezakati T, Tan A and Seifalian A M 2014 *J. Colloid Interface Sci.* **435** 145–55
[174] Tu C, Nagata K and Yan S 2017 *Polym. Bull.* **74** 1237–52
[175] Castelaín M, Martínez G, Marco C, Ellis G and Salavagione H J 2013 *Macromolecules* **46** 8980–7
[176] Hu H, Zhang G, Xiao L, Wang H, Zhang Q and Zhao Z 2012 *Carbon* **50** 4596–9
[177] Sabzi M, Jiang L, Liu F, Ghasemi I and Atai M 2013 *J. Mater. Chem.* A **1** 8253
[178] Yang J H, Lin S H and Lee Y D 2012 *J. Mater. Chem.* **22** 10805–15
[179] Zeng X, Yang J and Yuan W 2012 *Eur. Polym. J.* **48** 1674–82
[180] Noël A, Faucheu J, Rieu M, Viricelle J P and Bourgeat-Lami E 2014 *Compos. Sci. Technol.* **95** 82–8
[181] Mutlay B, Tudoran L B, Ibrahim M and Lucian Barbu T 2014 *Fullerenes Nanotubes Carbon Nanostruct.* **22** 413–33
[182] Vo N H, Dao T D and Jeong H M 2015 *Macromol. Chem. Phys.* **216** 770–82
[183] Lan Y, Liu H, Cao X, Zhao S, Dai K, Yan X, Zheng G, Liu C, Shen C and Guo Z 2016 *Polymer* **97** 11–9
[184] Liu N, Luo F, Wu H, Liu Y, Zhang C and Chen J 2008 *Adv. Funct. Mater.* **18** 1518–25
[185] Zhao P, Luo Y, Yang J, He D, Kong L, Zheng P and Yang Q 2014 *Mater. Lett.* **121** 74–7
[186] Chiu Y C, Huang C L and Wang C 2016 *Compos. Sci. Technol.* **134** 153–60
[187] Tu Z, Wang J, Yu C, Xiao H, Jiang T, Yang Y, Shi D, Mai Y W and Li R K Y 2016 *Compos. Sci. Technol.* **134** 49–56
[188] Vadukumpully S, Paul J, Mahanta N and Valiyaveettil S 2011 *Carbon* **49** 198–205
[189] Zha J W, Zhang B, Li R K Y and Dang Z M 2016 *Compos. Sci. Technol.* **123** 32–8
[190] Li Y, Tang J, Huang L, Wang Y, Liu J, Ge X, Tjong S C, Li R K Y and Belfiore L A 2015 *Compos. Part A: Appl. Sci. Manuf.* **68**
[191] Moriche R, Sánchez M, Jiménez-Suárez A, Prolongo S G and Ureña A 2016 *Compos. Part B: Eng.* **98** 49–55
[192] Monti M, Rallini M, Puglia D, Peponi L, Torre L and Kenny J M 2013 *Compos. Part A: Appl. Sci. Manuf.* **46** 166–72
[193] Meng Q, Wu H, Zhao Z, Araby S, Lu S and Ma J 2017 *Compos. Part A: Appl. Sci. Manuf.* **92** 42–50
[194] Li Y, Zhang H, Porwal H, Huang Z, Bilotti E and Peijs T 2017 *Compos. Part A: Appl. Sci. Manuf.* **95** 229–36
[195] Zhao S, Chang H, Chen S, Cui J and Yan Y 2016 *Eur. Polym. J.* **84** 300–12
[196] Tang G, Jiang Z G, Li X, Zhang H B, Hong S and Yu Z Z 2014 *Compos. Part B: Eng.* **67** 564–70
[197] Park O K, Hwang J Y, Goh M, Lee J H, Ku B C and You N H 2013 *Macromolecules* **46** 3505–11
[198] Park O K, Kim S G, You N H, Ku B C, Hui D and Lee J H 2014 *Compos. Part B: Eng.* **56** 365–71
[199] Luo Y, Zhao P, Yang Q, He D, Kong L and Peng Z 2014 *Compos. Sci. Technol.* **100** 143–51
[200] Yang H, Liu P, Zhang T, Duan Y and Zhang J 2014 *RSC Adv.* **4** 27687–90
[201] He C, She X, Peng Z, Zhong J, Liao S, Gong W, Liao J and Kong L 2015 *Phys. Chem. Chem. Phys.* **17** 12175–84
[202] Dong B, Wu S, Zhang L and Wu Y 2016 *Ind. Eng. Chem. Res.* **55** 4919–29
[203] Lin Y, Liu S, Peng J and Liu L 2016 *Compos. Sci. Technol.* **131** 40–7